Tu-Pos475

TWO DIMENSIONAL FINITE ELEMENT SIMULATION OF ELECTROPHORESIS AND SEDIMENTATION. ((**T.P. Moody**[1], H.K. Shepard[2] and T.M. Laue[1])) [1]Dept. of Biochemistry and Molecular Biology, [2]Dept. Of Physics, Univ. of New Hampshire, Durham NH 03824.

In a typical electrophoresis experiment, the electric field is assumed to be invariant with position in the device. Near walls that are parallel to the direction of the field, however, the strength of the field may vary. If the distance between such walls is sufficiently small, such edge effects may substantially affect transport. Similarly, in sedimentation, walls that are parallel to the gravitational field may interact with solution components and, in so doing, affect transport. Edge effects due to interactions between walls and components can also occur in electrophoresis. Again, the smaller the volume of the system, the more such edge effects will affect transport. A two dimensional version of the Claverie method is used to simulate transport in a system that exhibits edge effects. Transport in one dimension includes a flux due to the field and a flux due to diffusion, while that in the other, orthogonal dimension involves a flux due to diffusion alone. This latter flux is zero in the absence of edge effects. Simulation results are shown that may be relevant to novel analytical electrophoresis and analytical ultracentrifugation methods under development in our laboratory. Grant acknowledgments: NSF BIR-9314040, NSF DIR-9002027.

Tu-Pos476-Tu-Pos506

Reserved for High School Student Posters.

LOCAL Ca^{2+} SIGNALING IN MUSCLE AND NERVE

W-AM-SymI-1 **C. Franzini-Armstrong, University of Pennsylvania**
Clustering of Ryanodine Receptors and Dihydropyridine Receptors

W-AM-SymI-2 **I. Parker, University of California, Irvine**
Elementary Ca^{2+} Release from IP_3 Receptors

W-AM-SymI-3 **J. A. Connor, Lovelace Institutes**
Ca^{2+} Signaling in Neural Dendritic Spines

W-AM-SymI-4 **W. J. Lederer, University of Maryland, Baltimore**
Ca^{2+} Sparks in Muscle

MYOSIN I

W-AM-A1

SH1 AND SH2-MODIFIED MYOSIN HEADS ACTIVATE THE REGULATED ACTIN. ((**Andrey A. Bobkov***, Elena A. Bobkova[†], Earl Homsher[†] and Emil Reisler*)) *Dept. of Chem. & Biochem. and Molecular Biology Inst., UCLA, Los Angeles, CA 90095. [†]Dept. of Physiol., School of Medicine, UCLA, Los Angeles, CA 90025.

The reactive SH1 (Cys-707) and SH2 (Cys-697) groups of the myosin head (S1) can be selectively labeled and have been used as an attachment sites for either fluorescent or spin probes in solution and fiber experiments. It was shown in the *in vitro* motility assays with unregulated actin, that selective modification of SH1 or SH2 groups disrupts the motor function of myosin [Root & Reisler (1992) *Biophys. J.* **63**, 730-740]. In this study we examined the effect of SH1 and SH2-modified S1 on the motility of the regulated actin. N-ethylmaleimide (NEM), (N-1[1-oxyl-2,26,6-tetramethyl-4-piperidinyl]iodacetamide (IASL), (iodoacetamidoethyl)aminonaphthalene-1-sulfonic acid (IAEDANS) and iodoacetamide (IAA) were used to selectively modify SH1 group on S1. 4-[N-[(iodoacetoxy)ethyl]-N methylamino]-7-nitrobenz-2-oxa-1,3-diazole (IANBD) was used to selectively modify SH2 group on S1. Addition of S1 modified with any of these reagents to the *in vitro* motility assay solutions increased the percentage of regulated actin filaments moving over unmodified HMM and their sliding velocity at pCa 5, 7, and 8. Addition of unmodified S1 had no effect on actin sliding under the same conditions. Acto-S1 ATPase measurements showed that IASL-SH1-S1, IAEDANS-SH1-S1 and IANBD-SH2-S1 had significantly lower K_m than unmodified S1. This indicates that SH1 and SH2-modified S1 have higher than unmodified S1 affinity to actin in the presence of ATP. Overall, these results demonstrate that SH1 and SH2 modified S1 can activate the regulated actin. Such activation improves the efficiency of unmodified heads, increasing the percentage of moving actin filaments and their velocity in the *in vitro* motility assay.

W-AM-A2

Glu124-Arg149 OF THE REGULATORY LIGHT CHAIN IS LOCATED ON THE PHOSPHORYLATION SIGNALLING PATHWAY IN SMOOTH MUSCLE MYOSIN. ((Guanming Wu, A. Wong, & R.C. Lu)) Muscle Research Group, Boston Biomed. Res. Inst., Boston, MA 02114

Regulatory light chain mutants, RLC-C18 and RLC-C165, containing Cys at 18 and 165, respectively, labeled with benzophenone-4-iodoacetamide, were exchanged into myosin in their phosphorylated (P) or unphosphorylated (unP) forms. Previously we showed by SDS-PAGE that intrachain photocrosslinking in RLC-C18 occurs only in the unP state. In the case of RLC-C165, the yield of one of two crosslinked bands decreased significantly whereas the other was unaffected by phosphorylation (Qian et al., Biophys.J. 70, A3, 1996). Peptide mapping in conjunction with mass spectrometry showed that C165 crosslinks to a tryptic peptide A17-K34 which includes the phosphorylation site S19 and this crosslinking is unaffected by phosphorylation. We also found that two adjacent tryptic peptides in the C-terminal domain, E124-R132 and F133-R149, are crosslinkable to C165 as well to C18; however, crosslinking to these two peptides, whether from C18 or C165, is inhibited in the phosphorylated state. The results clearly showed that the proximity between C165 and the region containing the phosphorylation site is not affected by phosphorylation. On the other hand, phosphorylation changes the spatial relationship between the region of E124-R149 and the region containing both C165 and C18. In scallop myosin the region corresponding to E124-R149 is located at the interfaces between RLC and the essential light chain as well as the heavy chain (Xie et al., Nature, 368, 306, 1994). In light of this work our results indicate that the region containing E124-R149 is involved in the transmission of the phosphorylation signal to the rest of molecule via its contacts with the essential light chain and the heavy chain. Supported by NIH AR41637 & AR28401.

W-AM-A3

MYOSIN WITHOUT THE PUTATIVE "LEVER ARM" STILL GENERATES STEPS IN THE LASER TRAP

(William H. Guilford, Anne-Marie Lauzon, Yelena Freyzon*, David M. Warshaw and Kathleen M. Trybus*) University of Vermont, Burlington, VT 05405 and *Brandeis University, Waltham, MA 02254

A simple model has been proposed for generation of force and motion by myosin, commonly referred to as the "lever arm hypothesis" (Fisher *et al.*, 1995). In this model, a substantial portion of the myosin head maintains a fixed orientation relative to actin, while the light chain binding domain (the "neck region") pivots about a fulcrum near where the motor and light chain binding domains abut one another. The simplest lever arm model predicts that step displacements generated by myosin should scale linearly with neck length. We have demonstrated previously that myosin with an elongated neck generates greater unitary displacements (≈13 nm) in the laser trap (Guilford *et al.*, 1996). As an additional test of this model, we compared unitary displacements from smooth muscle HMM, and a mutant HMM without a neck region (neckless), both expressed in an insect cell line (Trybus, 1994). Neckless HMM produced smaller displacements (≈7 nm) compared to wild type HMM (≈10 nm), and the attached time of the former was longer in duration. While the decreased unitary displacement in general supports the lever arm hypothesis, the fact that displacements were not reduced to zero suggests a more complex system. Perhaps (a) the S-2 region substitutes as a lever arm, (b) the fulcrum lies nearer the actin binding site than previously believed, or (c) a second mechanism (*e.g.* hand-over-hand) is active in two-headed myosin.

W-AM-A4

SLOWER *IN VITRO* MOTILITY OF ACTIN FILAMENTS WITH ELEVATED SOLUTION VISCOSITY

((**P.B. Chase**, K. Kulin and T.L. Daniel)) Depts. of Radiology, Physiology & Biophysics, and Zoology, University of Washington, Seattle, WA 98195.

We recently demonstrated that elevated solution viscosity (η/η_0) decreased both shortening velocity (V_{US} or V_{max}) and the kinetics of isometric tension redvelopment (k_{TR}) of maximally Ca^{2+}-activated skinned fibers (Chase *et al* 1996. *Biophys J* 70:A41); both decreased in proportion to $(\eta/\eta_0)^{-1}$. To test the hypothesis that η/η_0 acts at the molecular level, rather than sarcomeric or cellular levels, we investigated motion of fluorescently-labeled F-actin in an *in vitro* motility assay at elevated η/η_0. Assays used chymotryptic-HMM on nitrocellulose-coated surfaces (30°C); care was taken to minimize effects of ATP-insensitive HMM (Regnier *et al* 1996. *Biophys J* Nov., in press). Viscosity of actin buffer (AB) was varied by adding either sucrose or fructose. Control speed was 7.2 μm s^{-1}. Speed varied in proportion to $(\eta/\eta_0)^{-1}$ (see Fig); this effect was not due to osmotic forces. At $\eta/\eta_0 = 6$, speed was slowest (by 35%) for long filaments although this length dependence was not observed at $\eta/\eta_0 = 2$ - 3 where speed was 40 - 50% of control. Our results (i) show that viscosity affects actomyosin function at the molecular level as well as in skinned fibers, and (ii) support the hypothesis that viscosity primarily affects crossbridge diffusion rather than filament sliding *per se*. (Supported by NIH grant HL52558)

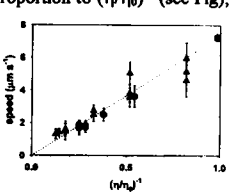

W-AM-A5

CONFORMATIONAL CHANGES IN MYOSIN MEASURED BY LUMINESCENCE RESONANCE ENERGY TRANSFER.

((**Paul R. Selvin**, Elise Burmeister Getz and Roger Cooke)) Lawrence Berkeley National Laboratory, Berkeley CA 94720 and UCSF, San Francisco, CA 94143.

We have measured distances between the neck and catalytic regions of myosin using luminescence resonance energy transfer. The technique extends the distance-range and accuracy of conventional fluorescence resonance energy transfer measurements. In the absence of actin, the distances are in agreement with the myosin crystal structure. In the presence of actin, the measurements indicate that myosin adopts a slightly more open configuration than without actin. Specifically, we find the distance between cys108 on gizzard light chain and cys707 in the catalytic domain to be 72Å in the rigor complex in the absence of actin. This distance increases to 76Å upon myosin binding to actin. We have also measured this distance as a function of nucleotide (ATP, ADP) and nucleotide analogs. The measurements support the notion that cys707 on the heavy chain is near, but not at, the fulcrum for myosin flexure. The measurements also indicate that a neck-swing occurs during the muscle powerstroke: fitting of the distances into the myosin crystal structure suggests a 24 degree neck-rotation and a 28 Å powerstroke, although the uncertainty in these numbers is large because cys707 is near the fulcrum.

W-AM-A6

MYOSIN AND PARAMYOSIN INTERACTION DURING THICK FILAMENT ASSEMBLY IN *C. ELEGANS*.

((**P.E. Hoppe** and R.H. Waterston)) Dept. of Genetics, Washington University School of Medicine, St. Louis, MO 63110

We are using a combination of molecular biology, cell biology, and genetics to study thick filament assembly in striated muscle. *C. elegans* body wall muscle contains two isoforms of myosin heavy chain, MHC A and MHC B, that perform functionally distinct roles within the thick filament (Miller et al., 1983, Cell 34, 477; Waterston, 1989, EMBO 8, 3429). In our current work we are studying myosin-paramyosin assembly by characterizing a unique genetic interaction between MHC A and a paramyosin mutant. Overexpresson of MHC A but not MHC B improves the structural defects and motility in animals homozygous for *e73*, a missense allele of paramyosin. Using chimeric myosins, we have found that this MHC A-specific suppression does not map to the 2 regions defined in our previous work as important for MHC A-specific filament initiation function (Hoppe and Waterston, 1996, JCB in press). Instead, the C-terminus of MHC A is essential for *e73* suppression, suggesting that suppression may involve a parallel myosin-paramyosin interaction that may occur by the same molecular stagger as that proposed for paramyosin-paramyosin association (Gengyo-Ando and Kagawa 1991, J Mol. Biol 219, 429). This parallel alignment model was based upon the positions of the *e73* mutation and its intragenic supressors (point mutations *m208* and *m209*) within the paramyosin rod. We are currently testing whether a similar parallel myosin-myosin interaction may occur by introducing the *e73* mutation and its intragenic suppressor mutation, *m209*, into homologous positions in the MHC A rod. In addition, to further elucidate wild-type assembly as well as the mechanism by which increased expression of MHC A suppresses *e73*, we have generated MHC A fused with green flouresecent protein (GFP) to visualize MHC A in living embryos. This GFP construct localizes correctly, rescues MHC A mutants, and suppresses *e73*, despite having apparently compromised contractile function. We are currently making 4-D movies to compare MHC A assembly behavior in wild-type, *e73*, and *e73*-suppressed backgrounds.

W-AM-A7

EXPRESSION OF SMOOTH MUSCLE MYOSIN ISOFORMS DURING URINARY BLADDER GROWTH AND HYPERTROPHY

((**M. DiSanto**, Z. Wang, R. M. Levin, and S. Chacko)) University of Pennsylvania, Philadelphia, PA 19104.

Hypertrophy of the smooth muscle cells in the urinary bladder alters the composition of smooth muscle myosin isoforms to those of the developing bladder. To determine whether any correlations exist between the fetal growth and compensatory hypertrophy, we investigated the expression of myosin heavy chain (MHC) and essential (17 kDa) light chain isoforms during growth and hypertrophy. Total RNA was isolated from bladder smooth muscle layers from 27-day fetuses, 3 day pups, normal adults, and adults that had been obstructed for 7 days and then reversed for 14 days. Using reverse transcriptase-PCR (RT-PCR), we investigated the expression of mRNA transcripts for smooth muscle myosin heavy chain (MHC) isoforms SM1 and SM2 (insertion at the C-terminal region) and the isoforms with insertion (7 amino acids) at the N-terminal 25kDa/50kDa (ATP-binding) region as well as expression of the essential light chain isoforms LC17a and LC17b using appropriate oligonucleotide primers. Hypertrophied bladders showed an increase in the mRNA transcript level for SM1 and a decrease for both SM2 and the N-terminal insert which returned to near normal upon reversal of the hypertrophy. During development, the MHC isoform composition changed from predominantly SM1 (70% N-terminal inserted) at 27 day gestation to an SM2:SM1 ratio of 2.8:1 (predominantly inserted) in the adult. Also during development, the amount of LC17a increased from 65% (27 day gestation) to 77% in the adult bladder but remained fairly constant during hypertrophy. Our results indicate that the levels of both SM2 and N-terminal insert are decreased both during hypertrophy of the adult bladder and during fetal growth. Supported by NIH Grants.

W-AM-A8

ACUTE QUADRIPLEGIA AND LOSS OF THICK FILAMENT PROTEINS AFTER TREATMENT WITH NON-DEPOLARIZING NEUROMUSCULAR BLOCKING AGENTS (NMB) AND HIGH DOSES OF CORTICOSTEROIDS IN INTENSIVE CARE UNIT PATIENTS.

((L. Larsson[1], X. Li[1], L. Edström[2], L. I. Eriksson[3], H. Zachrisson[1,3] and S. Schiaffino[4])) Dept. Clin. Neurophysiol.[1], Neurol.[2] and Anaesth.[3], Karolinska Hospital, Stockholm, Sweden and Center of Muscle Biol. & Physiopath.[4], Padova Univ., Italy

Almost 20 years ago MacFarlane and Rosenthal (1977) reported a case of acute quadriplegia affecting spinal nerve innervated muscles in a 24 year old woman after treatment with NMB and high doses of corticosteroids. In the past ten years more than 70 such cases have been reported, but the underlying mechanisms are not fully understood. The aim of this study was to investigate the cellular and molecular mechanisms underlying the acute quadriplegia. For this purpose, we have used cell-physiological, biochemical and molecular biological techniques to study contractile properties, expression of myofibrillar proteins and the regulation of myofibrillar protein synthesis and degradation. These measurements have been performed in parallel with electrophysiological studies of peripheral nerves and skeletal muscles, enzyme-histochemical and EM analyses of muscle samples from the paralysed muscles. In the acute stage there is a dramatic decrease or complete loss of thick filament proteins, a disorganization of the normal sarcomere structure and a complete loss of the force generating capacity at the single cell level. During recovery, myosin and myosin associated proteins are re-expressed resulting in generation of force upon Ca^{2+} activation of single muscle cells and a slow but gradual recovery of voluntary limb movements. In the acute stage, biochemical, electrophysiological and morphological analyses demonstrate a significant sarcolemmal defect. It is hypothesized that the acute quadriplegia is (1) initially caused by an inexcitable sarcolemma caused by NMB, corticosteroids and myositis, (2) followed by a block of myosin synthesis at the tranacriptional level, and (3) finally recovery of protein synthesis, incorporation of myosin and myosin associated proteins into the thick filament and a gradual improvement of skeletal muscle function.

W-AM-A9

NEURITE OUTGROWTH INVOLVES MYOSIN IIB BUT NOT MYOSIN IIA OR MYOSIN I

((Steve Wylie, Pei-jun Wu, Katalin A. Holland, Hitesh Patel, & **Peter D. Chantler**))
Molecular Biology Unit, Royal Veterinary College, University of London, U.K.

This laboratory has demonstrated previously that both myosin I and myosin II are localized immediately adjacent to the plasma membrane and at the leading edge of neuritic growth cones (Miller et al., 1992. *Neuron.* 8. 25-44; Li et al., 1994. *P.N.A.S.* 91. 853-857), suggestive of a functional role in neurite outgrowth. Here, we have used sequence information for myosins I, IIA and IIB to design isoform-specific sense and antisense oligonucleotides in order to test directly if these isoforms play any role in neuritic outgrowth and growth cone advance. Cultured mouse N2A cells were treated with sense or antisense oligos directed against isoform-specific sequences for myosins I, IIA and IIB, located within coding or non-coding sequence at the 5' end of the transcripts. Neurite outgrowth was monitored through measurement of the length and number of neurites per cell. Attenuation of myosin expression by antisense treatment was examined using primary antibodies directed against either myosin I or II, as appropriate. Anti-myosin I staining declined significantly in cells treated with antisense oligos directed against myosin I whereas fluorescence levels were unaffected in cells treated with sense oligos. However, no gross change in neurite outgrowth was observed suggesting that myosin I may not play a role in filopodial extension. Similarly, no decrease in neurite length or number was detected with either antisense or sense oligos directed against myosin IIA, or with sense oligos directed against myosin IIB. By contrast, antisense oligos directed against regions of myosin IIB dramatically attenuated neuritic process extension. This effect was shown to be reversible, neurite outgrowth being restored following cessation of the antisense regimen. RT-PCR will determine if the antisense oligo is acting to deplete cellular transcripts or to prevent their translation. Our results are consistent with the view that myosin IIB performs a direct role in facilitating filopodial extension of neuronal growth cones. Supported by grants from the Wellcome Trust and the B.B.S.R.C. to P.D.C.

NEW STRUCTURES: PROTEINS, COMPLEXES, VIRUSES

W-AM-B1

X-RAY CRYSTALLOGRAPHIC STUDIES ON NORWALK VIRUS CAPSIDS.

((B.V.V. Prasad[1], M. Hardy[2], R. McKenna[3],T. Dokland[3], M. Vyas[1], M. G. Rossmann[3]and M.K. Estes[2].)) [1]Dept. Biochem., [2]Div. Mol. Virol., Baylor Coll. Med., Houston, TX 77030; [3]Dept. Biological Sciences, Purdue Univ., W. Lafayette, IN 47907. (Spon. M..F. Schmid).

Norwalk virus, belonging to the family *Caliciviridae* is single-stranded positive sense RNA virus. It is the major cause of epidemic non-bacterial gastroenteritis in humans. This virus, which is exclusively a human pathogen, is unique among human viruses. The capsid is formed by one structural protein. Three-dimensional structure of the baculovirus-expressed Norwalk (rNV) capsids has been determined using three-dimensional electron cryo-microscopy to a resolution of 22 Å. These particles, 380 Å in diameter, exhibit T=3 icosahdral symmetry. Dimers of the capsid protein form distinct arch-like capsomeres at all the local and strict 2-fold axis. We have crystallized the intact rNV capsids suitable for atomic resolution structural analysis by X-ray crystallography. These crystals, diffract to ~3.2 Å resolution. Data collection has been carried out on the native crystals using synchrotron radiation source (F1, CHESS) at room temperature and also from a frozen crystal. Analysis of the oscillation photographs has indicated that the unit cell dimensions are 606 Å x 606 Å x 467 Å with a tetragonal space group. Phase extension using the cryoEM structure as the model has been carried out to a resolution of 4.2 Å and further phase extension to 3.2 Å resolution is in progress. This research is supported by R. Welch Foundation, NIH grants and W.M.Keck foundation.

W-AM-B2

A CARBOXYL-TERMINAL FRAGMENT OF BACTERIOPHAGE P22 SCAFFOLDING PROTEIN IS SUFFICIENT FOR PROCAPSID ASSEMBLY *IN VITRO*

((Matthew H. Parker[1], Sherwood Casjens[2], and **Peter E. Prevelige, Jr.**[1]))
[1]Dept. of Microbiology, Univ. of Alabama, Birmingham, AL [2]Dept. of Oncological Science, Univ. of Utah Health Science Center, Salt Lake City, UT

Salmonella typhimurium bacteriophage P22 is a useful model system for studying the assembly pathways of double-stranded DNA viruses. Assembly of P22 procapsids requires a 303-amino acid scaffolding protein, which exits upon DNA packaging into the phage head. While the carboxyl-terminal end of scaffolding protein interacts with phage coat protein, the amino terminal portion is believed to function mainly as an autoregulator of scaffolding protein synthesis. A scaffolding protein fragment was constructed, in which amino acids 1 through 142 were deleted. Removal of the amino-terminal portion allowed overexpression of the protein in *E. coli*. The purified carboxyl-terminal fragment catalyzes the *in vitro* formation of procapsid-like particles, as indicated by increases in light scattering, sucrose density gradient sedimentation, and electron microscopy. Procapsid assembly catalyzed by the fragment is faster than with equimolar amounts of the full-length scaffolding protein, and has no detectable lag phase. Analytical ultracentrifugation and chemical crosslinking show that the fragment exists in a monomer/dimer/trimer equilibrium, unlike the full-length scaffolding protein, which forms monomers, dimers, and tetramers. Circular dichroism (CD) of the fragment, like the full-length scaffolding protein, indicates a high degree of alpha helicity. Thermal unfolding of the fragment, monitored by CD, is fully reversable, and the midpoint for thermal denaturation is somewhat higher than for equimolar amounts of the full-length protein. Possible roles for the amino-terminal domain of P22 scaffolding protein are discussed in light of this information.

W-AM-B3

FOLDING INTERMEDIATES IN VIRUS ASSEMBLY: RAMAN DYNAMIC PROBE OF PROCAPSID MATURATION IN THE dsDNA PHAGE P22.

((**R. Tuma**, P.E. Prevelige, Jr. and G.J. Thomas, Jr.)) School of Biological Sciences, University of Missouri, Kansas City, MO 64110.

Assembly of icosahedral dsDNA viruses usually proceeds in two steps. A precursor shell or procapsid is first assembled with the aid of scaffolding subunits. Subsequently, at the time of DNA packaging, the procapsid expands and scaffolding protein is released. A well studied example is the *Salmonella* phage P22. To elucidate the mechanism of procapsid expansion, we have employed time-resolved Raman spectroscopy to investigate peptide NH → ND exchange dynamics of coat (gp5) and scaffolding (gp8) subunits in the following assembly states: (1) free scaffolding protein extracted from procapsid shells, (2) scaffolding within procapsid shells, (3) empty procapsid shells (PS), and (4) empty expanded shells (ES). The unhindered H/D exchange of gp8 both within and extracted from procapsid shells indicates unusual structural flexibility and a molten-globule-like native state. On the other hand, H/D exchanges of gp5 in both PS and ES differ dramatically from that of gp8 and from one another. Quantitative analysis of the results, which is facilitated by study of fully-deuterated subunits in PS and ES, shows that significant enhancement of exchange protection accompanies procapsid expansion. On the basis of these and related results, we propose a detailed mechanistic model for procapsid shell maturation in dsDNA virus assembly. [NIH Grant GM50776.]

W-AM-B4

BINDING SITES FOR NEUTRALIZING ANTIBODIES OF ROTAVIRUS VISUALIZED BY CRYO-ELECTRON MICROSCOPY AND IMAGE RECONSTRUCTION.

((M. Tihova, H. Greenberg, M. Yeager))* The Scripps Research Institute, 10550 N. Torrey Pines Rd., La Jolla, CA 92037. *Stanford University Medical Center, Stanford, CA 94304. (Spon. by M. Tihova)

Infection by rhesus rotavirus (RRV) requires attachment of the 87kDa hemagglutinin protein VP4 to target cells. Trypsin cleaves VP4 at ARG241 and ARG247 generating VP8* (27 kDa; AA 1-247) and VP5* (60 kDa; AA 248-776), which remain bound to the virus particle. This cleavage event enhances viral infectivity and facilitates viral entry into the cell. VP4 is a multi-domained protein forming 60 dimeric spikes that have a radial length of ~200Å with ~110Å projecting from the surface of the virus. Each spike has a bi-lobed head attached to a square-shaped body formed by two rods that have a slight left-handed helical twist. These rods merge with an angled, rod-like domain connected to a globular base ~85Å in diameter. We are using cryo-electron microscopy and image analysis to map the binding sites of two VP4 monoclonal antibodies (2G4 and 7A12) that neutralize rotavirus. 2G4 and 7A12 specifically bind to VP5* and VP8*, respectively. Cryo-images of RRV decorated with IgGs or Fab fragments were recorded at 0.8μm and at 2.6μm defocus. The fuzzy surface of the particles in the strongly defocused image confirmed successful decoration, and the 0.8μm defocused micrograph was used for image processing. The 3D density map of RRV decorated with 7A12 shows striking similarity to native rotavirus (T=13*l* symmetry, a rippled outer capsid surface, and the same number, size and distribution of surface holes). The current map reveals that a 7A12 Fab fragment binds to the side of each VP4 head domain. The structural information provided by the analysis of RRV-antibody complexes and the conformational changes that take place will be fundamental for understanding mechanisms of viral pathogenesis and may provide clues for the rational design of therapeutic strategies.

W-AM-B5

Three-Dimensional Studies of the Hook-Basal Body Complex from *Salmonella typhimurium* ((D. Thomas, **D. G. Morgan**, T. Shaikh and D. J. DeRosier)) Rosenstiel Basic Medical Sciences Research Center, Brandeis University, Waltham, MA 02254 (Spon. by D. Thomas)

All reconstructions of the *Salmonella typhimurium* basal body complex obtained by electron microscopy and image analysis have been *cylindrically symmetric*, meaning that the various rings and the rod are not divided azimuthally into subunits. This symmetry is a consequence of ignoring the azimuthal orientation of the various features in the structure and has been necessary for prior structural studies. To achieve a true 3D reconstruction of the bacterial flagellum, we have developed new methods to determine the azimuthal orientation of the basal body complex.

One approach is to use the known structure of the hook to determine the azimuthal orientation of the hook/basal body complex. Features of the basal body rigidly attached to the hook should have the same azimuthal orientation as the hook. Inclusion of this information during image analysis should produce a truely 3D reconstruction of the entire complex. Initial results indicate that the rod has a helical structure (confirming what has always been assumed). The MS and LP rings are smooth (indicating that azimuthal orientations are still not optimal), but various refinements are possible.

We have also investigated the 3D organization of the C ring. By analyzing both top views and side views, we determine that the C ring consists of about 30 subunits. Prospects of using the C ring portion of the images to determine orientation appear promising.

W-AM-B6

DYNAMIC PROPERTIES OF HUMAN HEAT SHOCK PROTEIN HSP10 ((**Samuel J. Landry***, Karol Maskos*, N. Kalaya Steede*, John Hunt#, Johann Deisenhofer#)) *Dept. Biochemistry, Tulane University School of Medicine, New Orleans, LA 70112 and #Howard Hughes Medical Institute and Dept. Biochemistry, University of Texas Southwestern Medical Center, Dallas, TX 75235

We are characterizing the structure and dynamics of the human mitochondrial heat shock protein, HSP10, by X-ray crystallography and NMR. Our studies focus on segments homologous to a highly disordered mobile loop and a metastable roof-β-hairpin that were previously identified in the *Escherichia coli* HSP10 GroES. The loop probably mediates regulatory interactions of HSP10 with HSP60, leading to increased cooperativity in HSP60 conformational changes and ATP hydrolysis during cycles of unfolded protein binding and release. The roof-β-hairpin closes a potential avenue for egress of a folding substrate protein. Interest in these flexible segments of HSP10 also arises from their coincidence with immunodominant epitopes and the possible role of HSP10 in immune regulation as early pregnancy factor. A preliminary X-ray crystal structure of HSP10 has been solved by molecular replacement using a single subunit of GroES as a probe. Heteronuclear nuclear magnetic resonance experiments were carried out on a uniformly ^{15}N-labelled HSP10. Standard ^{15}N-edited NMR techniques afforded complete assignment of the backbone amide ^{1}H and ^{15}N pairs of 18 amino acids which form a mobile loop (residues 21-38) and 4 amino acids which are part of the roof-β-hairpin (residues 52-60). The lack of electron density in the X-ray map of HSP10 for residues 21-38 and 52-60 suggest high mobility in these regions. The dynamic properties of HSP10 have been studied at temperatures 298 K, 308 K, and 318 K by using NMR spectroscopy to measure spin-lattice relaxation rate constants, spin-spin relaxation rate constants, and steady state nuclear Overhauser enhancements of the backbone ^{15}N nuclear spins. Our heteronuclear relaxation studies give direct evidence that these regions have a high degree of dynamic flexibility with respect to the overall tumbling of the HSP10 seven-mer.

W-AM-B7

CRYSTAL STRUCTURES OF *BACILLUS STEAROTHERMOPHILUS* ADENYLATE KINASE WITH BOUND Ap_5A REVEAL AN INTERMEDIATE LID POSITION AND A FULLY COORDINATED MG^{2+}. ((**Michael B. Berry** and George N. Phillips, Jr)) *W. M. Keck Center for Computational Biology*, Department of Biochemistry and Cell Biology, Rice University, Houston, TX 77005-1892

Five crystal structures of *Bacillus stearothermophilus* adenylate kinase with bound Ap_5A, $Mg^{2+}Ap_5A$, $Mn^{2+}Ap_5A$, Co^{2+}/Ap_5A, and Cd^{2+}/Ap_5A have been determined by X-ray crystallography to resolutions of 1.67 Å, 1.96 Å, 1.85 Å, 1.85 Å, and 2.25 Å, respectively. The protein's lid domain, which contains a zinc finger motif with bound Zn^{2+}, is partially open, being both rotated and translated away from bound Ap_5A. In the $Mg^{2+}Ap_5A$ and $Mn^{2+}Ap_5A$ structures, Mg^{2+} and Mn^{2+} demonstrate full octahedral coordination. Co^{2+}/Ap_5A and Cd^{2+}/Ap_5A structures demonstrate the presence of a cation trap, other than the Mg^{2+} binding site, at the front of the active site. The flexibility of the lid domain in the ternary state and its direct interaction with bound molecules in the active site suggest that it acts as an entropic regulator of catalytic turnover in adenylate kinases. The interactions of the magnesium-coordinated water molecules with the protein and Ap_5A phosphate chain illustrate their involvement in phosphate transfer.

W-AM-B8

COMPARISON OF OXIDIZED AND REDUCED FLUOROPHORE IN RECOMBINANT WILD-TYPE GREEN FLUORESCENT PROTEIN ((Fan Yang and George N. Phillips, Jr.)) Department of Biochemistry and Cell Biology, and the W.M. Keck Center for Computational Biology, Rice University, Houston, TX 77005-1892

The crystal structure of recombinant wild-type green fluorescent protein (GFP) has been solved to a resolution of 1.9 Angstroms by multiwavelength anomalous dispersion (MAD) phasing methods (Yang et al., Nature Biotechnology, Vol. 14, 1246-1251, 1996). The protein is in the shape of a cylinder, comprising 11 strands of β-sheet with an α-helix inside and short helical segments on the ends of the cylinder. This motif, with β-structure on the outside and α-helix on the inside, represents a new protein fold, which we have named β-can. The fluorophore is on the central α-helix and protected by the cylinder. Its structure is consistent with the formation of the aromatic system made up of cyclization between residues Ser65 and Gly67 coupled with oxidation of the Cα-Cβ bond of Tyr66. Here, we report the structure of recombinant wild-type GFP reduced by sodium dithionite. After two weeks of reduction by 20 mM dithionite, GFP crystals were almost bleached and diffracted to a resolution of 2.6 Angstroms. The green color reappeared after the crystal was exposed to air. As expected, the reduced GFP structure shows that the planarity of the fluorophore is disrupted by the reduction of the Cα-Cβ bond of Tyr66. No other significant structural changes appear. Our results confirm that the mechanism of formation of the fluorophore in GFP requires molecular oxygen to oxidize the Cα-Cβ bond of Tyr66.

Supported by Robert A. Welch Foundation, NIH and NSF grants

W-AM-B9

THE STRUCTURE OF THE MONOOXYGENASE DOMAIN OF PEPTIDYLGLYCINE α-AMIDATING MONOOXYGENASE. (S. T. Prigge, A. S. Kolhekar, B. A. Eipper and L. M. Amzel) Departments of Biophysics and Neuroscience, Johns Hopkins University School of Medicine, Baltimore, MD 21205. (Sponsored by L. M. Amzel)

Approximately 50% of mammalian bioactive hormones, neurotransmitters, and growth factors are peptides with a COOH-terminal carboxamide, generated by N-oxidative cleavage of a glycine-extended prohormone. A single bifunctional enzyme is responsible for catalyzing the α-amidation of these physiological regulators, many of which are inactive without α-amidation. Peptidylglycine α-amidating monooxygenase (PAM) (EC 1.14.17.3) catalyzes two reactions at two separable catalytic domains: the first domain, peptidylglycine α-hydroxylating monooxygenase (PHM), catalyzes the copper, ascorbate, and molecular oxygen dependent α-hydroxylation of peptidylglycine substrates; the second domain, peptidyl-α-hydroxyglycine α-amidating lyase (PAL), is required to generate α-amidated peptide product and glyoxylate. The catalytic core of the PHM domain (residues 42-356 of rat PAM) has been crystallized in the orthorhombic space group P212121 with cell dimensions a=68Å, b=70Å, c=81Å, and α=β=γ=90°. Multi-wavelength anomalous dispersion (MAD) data has been collected around the copper absorption edge at the National Synchrotron Light Source and the Stanford Synchrotron Radiation Laboratory. Data out to 2.3Å has been phased using the MADSYS package and structure determination is in progress.

W-AM-C1

ORK1, a K^+-selective leak channel cloned from *D. melanogaster* by expression in *S. cerevisiae*, a member of a new 2 P domain K^+ channel family.

((**Steve A. N. Goldstein***, Laura A. Price, David N. Rosenthal* and Mark H. Pausch))
*Departments of Pediatrics and Cellular and Molecular Physiology, Yale University School of Medicine, New Haven, CT. 06536-0812 and Cyanamid Agricultural Research Center, Box 400, Princeton, NJ 08543-0400.

A K^+ channel gene has been cloned from *D. melanogaster* by complementation in *S. cerevisiae* cells defective for K^+ uptake. Found in neuromuscular tissues of adult flies, heterologous expression in yeast confers K^+ transport capacity. In *Xenopus laevis* oocytes, expression yields an ungated K^+-selective current whose attributes resemble the 'leak' conductance thought to mediate the resting potential of vertebrate myelinated neurons but whose molecular nature has long-remained elusive. The predicted protein has two pore (*P*) domains and four membrane-spanning helices and is a member of a new K^+ channel family. Expression of the channel in flies and yeast cells makes feasible studies of structure and *in vivo* function using genetic approaches that are not possible in higher animals.

Gene expression in *X. laevis* oocytes bathed in physiological solutions yields K^+-selective currents that are instantaneous with changes in voltage and outwardly-rectifying. Increased external K^+ concentration (K_O) significantly alters this current-voltage relationship; as K_O rises, rectification is lost and K^+ ions flow inward at hyperpolarized potentials. This sensitivity to K_O appears intrinsic to the channel as it approximates expectations from constant field theory for simple electrodiffusion through an open K^+- selective pore. The new gene and its product have been named ORK1, as an abbreviation for Open Rectifier K^+ channel.

W-AM-C2

A NEW FAMILY OF POTASSIUM CHANNELS: RELATIVES OF VOLTAGE AND CALCIUM ACTIVATED MAXI K CHANNELS.

((**M. Wallner**, P. Meera and L. Toro)) Dept. of Anesthesiology, UCLA, Los Angeles, CA 90095-1778, USA.

The unique tail region of MaxiK channels, which is the highest conserved part between mammalian MaxiK channels and the *Drosophila* homolog, was used for database searches. We identified a homologous *Caenorhabditis elegans* cDNA sequence, predicted from a genomic sequence (Sanger Centre, UK), with an overall protein sequence similarity of 48% (22% identity) with mammalian MaxiK channels. Besides the overall homology, the most remarkable feature is the high sequence identity in the pore region, suggesting that this *C. elegans* sequence indeed encodes a potassium channel. Hydrophibicity analysis and sequence alignments show that this *C. elegans* sequence is unique upstream of homology region S5; e.g. no conserv positive charges in the S4 region. Expressed Sequence Tag (EST) database searches with this predicted C. elegans sequence revealed three *C. elegans* cDNA-clones (Y. Kohara. National Institute of Genetics, Japan) derived from the above mentioned genomic sequence, and a homologous human cDNA clone (WashU-Merk EST project). We obtained these clones (from Y. Kohara and the ATCC) and confirmed - with minor corrections - the predicted *C. elegans* cDNA sequence. The human EST clone was sequenced completely. The conceptual translation of the human EST-clone shows 63% protein sequence similarity (44% identity) with the *C. elegans* clones. The human clone was also used for Northern Blot analysis which revealed a band of about 4.4 kb in a variety of tissues with the highest mRNA levels in heart and skeletal muscle. We are currently working to complete these partial sequences for functional expression studies.
(Supported by NIH grant HL54970, LT is an AHA Established Investigator).

W-AM-C3

MOLECULAR DESCRIPTION OF *cSlo*, A Ca^{2+}-ACTIVATED K^+ CHANNEL EXPRESSED IN THE CHICKEN'S BRAIN AND INTERNAL EAR.

((**Kevin P. Rosenblatt**, Z.-P. Sun, and A. J. Hudspeth)) Howard Hughes Medical Institute and Laboratory of Sensory Neuroscience, Rockefeller University, New York, NY 10021.

In the internal ears of many vertebrates, hair cells are frequency-tuned by electrical resonance. This tuning process is dependent on the interplay of ionic channels of two types: voltage-dependent, non-inactivating Ca^{2+} channels and large-conductance, Ca^{2+}-activated K^+ channels. The number and single-channel kinetics of these K^+ channels largely govern a cell's frequency selectivity and thus establish an auditory organ's tonotopic map. The molecular mechanism underlying the variation in these channel properties, however, is not understood.

To investigate the molecular basis of electrical tuning in hair cells of the chicken's cochlea, we used the polymerase chain reaction (PCR) to generate cDNAs partially encoding the chicken's Ca^{2+}-activated K^+ channel. To obtain a full-length cDNA, we then screened a chicken-brain cDNA library with PCR-derived probes. A full-length clone of approximately 4 kilobases was assembled, sequenced, and found to imply 94% amino-acid identity with *hSlo*, the human brain homologue. Numerous alternatively spliced isoforms were detected during the cloning of *cSlo* from the chicken's brain; in addition to some novel exons, several previously known alternative exons were found to be expressed within the chicken's sensory epithelium.

Using *in situ* hybridization and the *in situ* PCR, we have demonstrated that *cSlo* is expressed within cochlear hair cells but not supporting cells. Reverse transcription-PCR analysis on localized patches of sensory epithelium and on isolated hair cells has confirmed the mRNA expression of both *cSlo* mRNA and several *cSlo* isoforms. We are now mapping in detail the distribution of *cSlo* variants. To determine the functional consequences of alternative splicing in cochlear hair cells, we are additionally examining the physiological properties of *cSlo* and certain of its variants in a heterologous expression system.

This research was supported by HHMI and by NIH grant DC00317.

W-AM-C4

CLONING A CARDIAC SPECIFIC ISOFORM OF HERG FROM THE MOUSE.

((**Barry London**, * Anita K. Beyer,* Kimberly P. Newton,* Matthew C. Trudeau,# and Gail A. Robertson#)) *Div. of Cardiology, University of Pittsburgh Medical Center, Pittsburgh , Pennsylvania 15213 and #Dept. of Physiology, University of Wisconsin School of Medicine, Madison, Wisconsin 53706.

Mutations of the human ether-a-gogo related gene (HERG) cause the autosomal dominant long QT syndrome in families linked to the LQT2 locus (Curran et al., 1995). Isolation of additional cardiac isoforms of HERG will aid in the search for mutations which cause the disease, and may improve our understanding of the mechanism by which the mutations lead to disease. We therefore sought to identify additional members of the HERG family in the mouse. We cloned MERG1, the mouse homolog of HERG, from genomic and cardiac cDNA libraries. We first identified MERG1a, the isoform homologous to the previously published HERG cDNA clone. It is 4.2 KB in length, comprised of 15 exons, and has an open reading frame 1162 amino acids in length with 96% identity to HERG. MERG1a is expressed at high levels in heart, brain, and testes by Northern blot analysis. We also identified a shorter isoform, MERG1c, and confirmed its existence by RACE of mouse heart cDNA. MERG1c is 3.2 KB in length, comprised of 11 exons, and begins at an alternate transcription initiation site in the MERG1 gene. It contains an open reading frame 820 amino acids in length, with almost the entire N-terminal domain of MERG1a replaced by 36 novel amino acids. MERG1c is expressed abundantly only in the heart.

Expression of MERG1a in *Xenopus* oocytes results in currents with properties similar to HERG and cardiac I_{Kr}. Coexpression of MERG1a with MERG1c produces channels with altered deactivation kinetics (Trudeau et al., this vol.). Thus, expression of a cardiac specific isoform of MERG1 may determine the properties of I_{Kr} in the heart.

W-AM-C5

EXPRESSION OF HERG HOMOLOGS CLONED FROM THE MOUSE

((**Matthew C. Trudeau**, Barry London,* Anita K. Beyer,* Kimberly P. Newton* and Gail A. Robertson)) Department of Physiology, University of Wisconsin Medical School, Madison, WI 53706 and *Division of Cardiology, University of Pittsburgh Medical Center, Pittsburgh, PA 15213.

A mouse homolog of the *human ether-a-go-go-related gene* (*HERG*) has been cloned and several splice variants of this locus have been characterized (London et al., this vol.). Expression of the MERG1a isoform, which differs from HERG by only 50 amino acids, produces a potassium current with properties very similar to those of HERG (Sanguinetti et al., Cell 81:299, 1995; Trudeau et al., Science 269:92, 1995). The MERG1a I-V relation has a region of negative slope at voltages positive to -10 mV, and a g-V relation with a half-point of -31 ± 0.3 mV and a slope of 7.6 ± 0.2 mV/e-fold change in conductance (n=5). MERG1a inactivates with a time constant of 8.0 ± 2.1 ms at 20 mV and deactivates with a time constant of 405 ± 91 ms at -100 mV. The current is blocked by the class III antiarrhythmic E-4031 with an IC_{50} of 600 nM.

Cardiac-specific MERG1c, an isoform lacking most of the N terminus, did not produce currents when expressed alone suggesting that homomeric assemblies of MERG1c are nonfunctional under these experimental conditions. However, when MERG1c was coexpressed with MERG1a, the resulting currents exhibited deactivation kinetics that were three-fold faster than those observed with the MERG1a homomers (τ = 122 ± 10 ms; n=8). Inactivation rate was not appreciably altered, nor was the voltage dependence of activation. These results are consistent with previous studies showing that HERG currents exhibit faster deactivation when the N terminus is deleted (Spector et al., 1996; Schonherr and Heinemann, 1996), and suggest that subunits lacking much of the N terminus coassemble with full-length subunits in Xenopus oocytes. Furthermore, they suggest that ERG N terminal splice variants may be important molecular determinants of cardiac I_{Kr} function.
Supported by NIH grant HL55973 (to G.A.R.) and an AHA-WI fellowship (to M.C.T).

W-AM-C6

HERG and minK: PHYSICAL AND FUNCTIONAL INTERACTIONS.

((**Thomas V. McDonald**, Zhen Ming, Zhihui Yu, Marian Meyers, Steve A. N. Goldstein* and Glenn I. Fishman)) Albert Einstein College of Medicine, Bronx, NY 10461 and *Yale University School of Medicine, New Haven, CT 06536.

The minimal K^+ channel protein (minK) is widely expressed in a variety of tissues and controversy exists over its role as a structural or regulatory ion channel subunit. Some speculate that minK underlies a slowly-activating delayed rectifier K^+ current in the heart, I_{Ks}. Others suggest it influences the rapidly-activating, delayed rectifier K^+ current (I_{Kr}) mediated by *HERG*, the human K^+ channel gene linked to a form of inherited long QT syndrome. To directly test for functional interaction between minK and *HERG* the two proteins were expressed in Chinese hamster ovary (CHO) cells. CHO cells stably expressing *HERG* demonstrate voltage-gated K^+ currents recognizable as I_{Kr} by whole cell patch clamp. While wild-type minK expressed alone shows no voltage-activated K^+ currents (10 cells), its expression in *HERG*-expressing CHO cells leads to a 2-fold increase in I_{Kr} density (maximal tail currents: 12.88 ± 1.6 pA/pF for *HERG* alone (n=55), 24.02 ± 3.45 pA/pF for minK plus *HERG* (n=39)). Notably, a mutant of minK (D77N), which passes no current despite reaching the plasma membrane in oocytes, does not increase I_{Kr} current (37 cells). Voltage-activation curves, current-voltage curves, and kinetics of activation and deactivation for I_{Kr} were not affected by co-expression of either minK. To test for a physical association of the two proteins, epitope-tagged minK (HA) and *HERG* (myc) constructs were co-expressed in COS cells. Immunopreceipitation (IP) with HA and visualization on Western blots by anti-myc (or IP with myc and staining with anti-HA) indicated that *HERG* and minK are tightly-associated and co-purify. Pulse-chase metabolic labeling of *HERG* does not suggest that minK acts to increase the half-life of the protein. These results provide evidence that minK subserves a regulatory role for I_{Kr} and implicate it in human cardiac arrhythmias.

W-AM-C7

ELECTROPHYSIOLOGICAL AND PHARMACOLOGICAL PROPERTIES OF HERG CHANNELS IN A STABLY TRANSFECTED HUMAN CELL LINE. ((**Z. Zhou**, Q. Gong, B. Ye, Z. Fan, J.C. Makielski, G.A. Robertson and C.T. January)) Departments of Medicine and Physiology, University of Wisconsin, Madison, WI.

We have obtained high efficiency expression of HERG channels in a stably transfected human embryonic kidney cell line. Northern blot analysis showed that the transfected cells expressed a 4.0 kb mRNA which is not expressed in non-transfected cells. Membrane potential and current were recorded at 35°C using whole cell patch clamp method. Transfected cells had a resting membrane potential of -56±1 mV (n=10). With depolarizing steps (K_o=4 mM), HERG current exhibited inward rectification with peak outward current (400-1700 pA) at voltages between -10 and 0 mV. The current density at 0 mV was 53.4±6.5 pA/pF (n=10). The threshold of current activation was about -50 mV. The half-maximal activation and slope factor of the activation curve were -25.9±2.0 mV and 6.0±0.3, respectively. The current was completely blocked by 300 nM E-4031. The dose response curve for E-4031 block showed an apparent Kd of 7.7 nM and Hill coefficient of 1.0. Cardiac action potential clamp was used to study the contribution of HERG current during an action potential. Under action potential clamp HERG current activated rapidly during the peak of the action potential and then increased slowly during repolarization with peak current obtained at voltages between -15 and -35 mV. These results demonstrate high efficiency expression of HERG channels and suggest that HERG may contribute repolarizing current throughout much of the cardiac action potential, particularly later phases of action potential repolarization.

W-AM-C8

SINGLE-CHANNEL PROPERTIES, DISTRIBUTION AND FUNCTIONS OF NA^+-ACTIVATED K^+ CHANNELS IN THE SOMA OF RAT MOTONEURONES ((B. V. Safronov & W. Vogel)) Physiologisches Institut, Justus-Liebig-Universität Giessen, Aulweg 129, 35392 Giessen, Germany

Na^+-activated K^+ (K_{Na}) channels were studied in the soma of motoneurones in spinal cord slices of new-born rat. Single-channel conductance was 139 pS in 155 mM K^+_o //85 mM K^+_i solutions. K_{Na} channels were voltage-independent and needed relatively high Na^+_i concentrations to become active, EC_{50}=39.9 mM. Li^+ could not substitute for Na^+ in activation of K_{Na} channels. The channels were predominantly found in the vicinity of cell processes, in the regions of most probable accumulation of cytoplasmic Na^+.

In current-clamp experiments, the shape of the single action potential (AP) recorded in Ca^{2+}-free Ringer was not changed after a substitution of external Na^+ with Li^+. However 0.4-0.8 s trains of APs were followed by a slow (1-2 s) afterhyperpolarization (sAHP) which reversibly disappeared when external Na^+ was replaced by Li^+. Na^+-activated sAHP persisted after addition of ouabain and its amplitude was even increased in K^+-free Ringer. sAHP disappeared when membrane potential was equal to K^+ equilibrium potential (E_K). This indicated that sAHP resulted from activation of Na^+-dependent K^+ conductance, rather than from activation of the electrogenic Na^+-K^+ pump.

We conclude that K_{Na} channels can play an important role in excitability of motoneurones. K_{Na} channels do not make a contribution to the single AP, but they are activated by a local accumulation of Na^+_i during trains of APs. Na^+-activated K^+ conductance can reduce membrane excitability and contribute to regulation of AP firing in motoneurones.

W-AM-C9

LARGE-SCALE PURIFICATION AND CHARACTERIZATION OF A *STREPTOMYCES LIVIDANS* K^+ CHANNEL. ((**L. Heginbotham**, E. Odessey, and C. Miller)). HHMI and Department of Biochemistry, Brandeis University, Waltham, MA 02254.

Direct structural work on K^+ channels has been plagued by an inability to purify sufficient protein. Historically the problem has been finding or developing a suitable source of channel protein; there is a dearth of naturally-occurring high-abundance sources, and high-level expression of functional protein in cultured cells has proven difficult. However, the recent identification of a K^+ channel from *Streptomyces lividans* may eliminate this problem (Schrempf, et al. (1995) *EMBO.* **14**: 5170.). This channel contains a P-region homologous to those of other K^+ channels, and can be produced in milligram quantities in *E. coli*. Since the protein is relatively small (161 amino acids), it is open to investigation by multiple structural techniques.

We constructed a synthetic gene for the channel based on its published amino acid sequence. When expressed in *E. coli*, the channel can be purified to homogeneity using an N-terminal 6xHis tag with a yield of approximately 0.5 mg/liter culture; a C-terminal streptavidin tag allows identification on western blots. The subunit composition of the purified channel is being investigated using a combination of tandem dimer constructs and coexpression experiments. We are using ^{86}Rb flux assays to assess the activity of the purified channel, and have begun attempts to form 2-D crystals for study by electron microscopy.

CARDIAC ELECTROPHYSIOLOGY II

W-AM-D1

HIGH AFFINITY BLOCK OF HERG CHANNELS BY AN ASTEMIZOLE METABOLITE, DESMETHYLASTEMIZOLE. ((**Z. Zhou**, Q. Gong, V.R. Vorperian and C.T. January)) Dept of Medicine, Univ of Wisconsin, Madison, WI.

QT interval prolongation and torsades de pointes occur with the selective H_1-receptor antagonist drug astemizole. We have recently demonstrated that the astemizole metabolite, desmethylastemizole (DM), blocks with high affinity the rapidly activating delayed rectifier K^+ current (I_{Kr}) in rabbit ventricular myocytes, which caused action potential prolongation and the induction of early afterdepolarizations. In the present study, we investigated the effect of DM on HERG channels stably expressed in HEK293 cells. HERG current is very sensitive to DM. At 1 nM, K^+ current through HERG was reduced by 48±4 % (n=4), and at 100 nM, the current was completely blocked. The dose response relationship (from 0.3 nM to 100 nM DM) yielded an apparent Kd of 1.0 nM and a Hill coefficient of 0.97. Block of current through HERG by DM depends on channel opening. With 30 nM DM present, with the first depolarizing step (to 0 mV) the peak current amplitude was unchanged and it then decayed with a time constant of 1.9 ± 0.1 sec (n=3). For control conditions current decayed minimally. Our data show that DM blocks HERG channels with high affinity. The affinity of DM for HERG is close to that previously shown for DM block of rabbit I_{Kr}. Since astemizole undergoes rapid first-pass metabolism predominantly to DM, our results may provide further insight into the mechanism of the proarrhythmic effects observed with astemizole in humans.

W-AM-D2

WITHDRAWAL OF ACETYLCHOLINE ELICITS Ca^{2+}-INDUCED DELAYED AFTERDEPOLARIZATIONS IN CAT ATRIAL MYOCYTES. ((Y.G. Wang, J. Hüser, L.A. Blatter and **S.L. Lipsius**)) Loyola University Medical Center, Maywood, IL 60153.

In atrial myocytes, withdrawal of acetylcholine (ACh) stimulates Ca^{2+} influx via L-type Ca^{2+} current ($I_{Ca,L}$) and Ca^{2+} uptake into sarcoplasmic reticulum (SR) via rebound stimulation of cyclic AMP (cAMP). The present study was designed to determine whether withdrawal of ACh can elicit Ca^{2+}-induced delayed afterdepolarizations (DADs). A perforated patch whole cell technique recorded voltage and ionic currents, and fluorescence microscopy (indo-1) measured alterations in intracellular free Ca^{2+} concentration ($[Ca^{2+}]_i$). Electrically stimulated atrial myocytes were exposed to 1 μM ACh for 1-2 min. Withdrawal of ACh elicited an transient increase in action potential duration, positive shift in plateau voltage, development of DADs and spontaneous action potentials. In addition, withdrawal of ACh elicited rebound stimulation of $I_{Ca,L}$ (+45%), Na/Ca exchange current ($I_{Na/Ca}$)(+16%), the development of transient inward currents (I_q) and the appearance of spontaneous $[Ca^{2+}]_i$ transients. Rp-cAMPs (50-100 μM) or H-89 (2 μM), inhibitors of cAMP-dependent protein kinase A, abolished DADs and spontaneous action potentials, rebound stimulation of $I_{Ca,L}$ and $I_{Na/Ca}$, the development of I_q and the appearance of spontaneous $[Ca^{2+}]_i$ transients elicited by withdrawal of ACh. We conclude that rebound stimulation of cAMP elicited by withdrawal of ACh can Ca^{2+} overload the SR and thereby lead to spontaneous SR Ca^{2+} release, stimulation of $I_{Na/Ca}$ and subsequent DADs. These mechanisms may contribute to triggered and/or spontaneous atrial depolarizations elicited by withdrawal of vagal nerve activity. Support by NIH grants HL27652 & HL51941.

W-AM-D3

CYTOCHALASIN D ALTERS RELATIONSHIP BETWEEN SWELLING-ACTIVATED CHLORIDE CURRENT AND CARDIAC MYOCYTE SIZE.

((**Ramesh Gopal** and Robert E. Ten Eick)) Department of MPBC, Northwestern University, Chicago, IL 60611.

Cardiac myocyte swelling occurs in a variety of pathological processes such as myocardial ischemia, infarction and reperfusion. We have found that osmotic swelling activates an outwardly rectifying chloride current ($I_{Cl\text{-}swell}$) in feline ventricular myocytes and that there is a linear relationship between the cross-sectional area of the phase-contrast microscopic image of the myocyte profile and the magnitude of $I_{Cl\text{-}swell}$. This relationship holds both when myocytes swell in hypotonic solution as well as when they shrink in hypertonic solution. The plot of current (ordinate) versus area (abscissa) provides a useful tool to investigate $I_{Cl\text{-}swell}$. We have used the current-area plot to study the role of the cytoskeleton in the regulation of $I_{Cl\text{-}swell}$. When myocytes were incubated overnight in cytochalasin D (15 μg/ml) and then subjected to hypotonic solution, $I_{Cl\text{-}swell}$ still occurred. However, the current-area plot no longer displayed the typical, linear relationship. In contrast, when myocytes were incubated with colchicine, the current-area plot was linear and unchanged from that of control myocytes. These findings suggest that $I_{Cl\text{-}swell}$ is importantly influenced by the f-actin cytoskeleton. We also found that a very modest sized $I_{Cl\text{-}swell}$ can depolarize cardiac myocytes, decrease the duration and alter the shape of the action potential. This finding implies that $I_{Cl\text{-}swell}$ may have an important role in the initiation and perpetuation of cardiac rhythm disturbances during ischemia and reperfusion and in hypertrophic hearts.

W-AM-D4

CROSS-REGULATION OF CARDIAC (EXON 5-) CFTR CHLORIDE CHANNELS BY PKA AND PKC IN *XENOPUS* OOCYTES.

((**J. Yamazaki**, M.L. Collier, B. Horowitz, and J.R. Hume)) Department of Physiology & Cell Biology, University of Nevada School of Medicine, Reno, NV 89557-0046.

The cardiac isoform (exon 5-) of cystic fibrosis transmembrane conductance regulator (CFTR) Cl^- channels has a high degree of conservation of putative PKA and PKC phosphorylation sites, but is missing 2 PKC phosphorylation sites on exon 5. Our objective was to investigate the regulation of cardiac CFTR Cl^- channels by PKC phosphorylation. *Xenopus* oocytes were injected with cRNA encoding the cardiac CFTR Cl^- channel 3-4 days prior to voltage clamp experiments. Oocytes were studied in both Ca^{2+}-free and Ca^{2+}-containing (niflumic acid, 100 μM) external solutions. Phorbol 12,13-dibutyrate (PDBu, 100 nM), 1,2-dioctanoyl-*sn*-glycerol (DiC_8, 100 μM) or a 'cAMP cocktail' (forskolin, 3-isobutyl-1-methylxanthine and 8-bromo-cAMP) activated time-independent Cl^- currents. PKC-activated currents were considerably larger in amplitude in Ca^{2+}-containing solutions (+70 mV; cAMP, 5053±527 nA, n=8; PDBu, 3389±513 nA, n=8), compared to Ca^{2+}-free solutions (+70 mV; cAMP, 4377±447 nA, n=20; PDBu 1449 ±273 nA, n=7), suggesting involvement of a Ca^{2+}-dependent PKC isoform. In contrast to Cl^- currents activated by PKA, PKC-activated currents were transient, with initial activation followed by inactivation and were inhibited by staurosporine (1 μM) and bisindolylmaleimide (5 μM). With submaximal concentrations, co-activation of both pathways resulted in larger currents than currents activated by PKA alone (cAMP+PDBu, 5571±754 nA; cAMP 4530±632 nA; n=5), however maximal PKA activation occluded further activation by PKC, but resulted in inactivation of the PKA activated currents. These results indicate: (1) PKA and PKC effects on cardiac CFTR Cl^- channels are additive but distinct in terms of inactivation properties and Ca^{2+}-dependence, and (2) PKC induces inactivation of CFTR Cl^- channels activated by either pathway. (supported by NIH HL 52803).

W-AM-D5

REPLACEMENT BY HOMOLOGOUS RECOMBINATION OF THE *MINK* GENE WITH *LACZ* REVEALS CELL-SPECIFIC *MINK* EXPRESSION.

((**Sabina Kupershmidt**,* Margaret Sutherland,* Dana King,** Mark A. Magnuson,** and Dan M. Roden*)) Vanderbilt University School of Medicine, Depts. of *Pharmacology and of **Molecular Physiology & Biophysics, Nashville, TN 37232-6602.

Expression of the *minK* gene in *Xenopus* oocytes evokes a slowly-activating, voltage-dependent, K^+-selective current that closely resembles the cardiac delayed rectifier I_{Ks}. However, the *in vivo* role of *minK*, and the hypothesis that *minK* forms functional K^+ channels by itself, remain controversial. We have therefore generated *minK* knockout mice in which the entire *minK* coding region has been deleted and replaced by the bacterial *lacZ* reporter gene, whose expression is controlled by endogenous *minK* regulatory elements. (+/-) mice have no obvious phenotype, while (-/-) mutants exhibit pronounced hyperactivity, head tossing, and circling movement; they also appear to be deaf. Electrocardiograms in (-/-) appear normal, and (-/-) x (-/-) breedings have resulted in term pregnancies. In (-/-) and (+/-), but not (+/+), mice, *lacZ* staining has been detected in lymph nodes and in restricted regions of kidney, brain, and heart in adults, and in the midbrain, heart, otic vesicle, and eye in 11-day embryos. Previous studies have shown that the abundance of *minK* mRNA transcripts in mouse heart is high in the embryo and but very low in adults. In adult mutant mouse hearts, intense *lacZ* staining is unexpectedly detected, but is restricted to the low atrial septum and the region of the AV node and proximal bundle of His. *In situ* hybridization has confirmed that *minK* is expressed in this highly restricted fashion. In the embryo, *minK* expression, both by *lacZ* staining and *in situ* hybridization, is present in the basal ventricle and outflow tract, but not in atrium. While the functional consequences of this restricted pattern of expression will require further evaluation, an important implication of these findings is that studies of cellular electrophysiology in genetically-modified animals will require markers for cell-specific expression of individual cardiac ion channel genes.

W-AM-D6

PARTIAL CELLULAR UNCOUPLING REVERSES UNIDIRECTIONAL CONDUCTION BLOCK ACROSS ABRUPT EXPANSIONS OF CARDIAC TISSUE.

((**S. Rohr**, J.P. Kucera, V.G. Fast and A.G. Kléber)) Dept. of Physiology, U. of Bern, Buehlplatz 5, CH-3012 Bern, Switzerland.

It is well known that unidirectional conduction block (UCB) due to current-to-load mismatch can occur at abrupt expansions of cardiac tissue and it has been hypothesized that the degree of electrical cell-to-cell coupling can affect this type of conduction disturbance.

We tested this hypothesis in patterned cultures of neonatal rat ventricular myocytes using multiple site optical recording of transmembrane voltage (MSORTV). Abrupt tissue expansions consisted of 50 μm to 70 μm wide cell strands merging with rectangular cell monolayers (≥ 2.2 x 2.2 mm). Transmembrane action potentials were simultaneously measured at up to 80 sites (spatial resolution = 50 μm) using the fluorescent voltage-sensitive dye di-8-ANEPPS. Electrical cell-to-cell coupling was reduced by local superfusion of the site of the expansion with 10 μM palmitoleic acid (PA).

In 5 preparations with UCB due to current-to-load mismatch under control conditions, superfusion with PA for 7 minutes produced total uncoupling. After 2 - 4 minutes of washout leading to partial recovery of cellular coupling, successful bidirectional conduction was observed in all preparations. At this time, slow but successful anterograde activation invaded the expansion either homogeneously (n = 3) or followed a tortuous pathway (n = 2). In addition, partial uncoupling also slowed retrograde conduction in the region of the tissue undergoing superfusion. After 10 minutes of washout, UCB (anterograde block and fast retrograde conduction) was reestablished in all preparations.

Thus, even though partial cell-to-cell uncoupling decreases conduction velocity, it can convert unidirectional conduction block to bidirectional conduction at abrupt tissue expansions. This suggests that cellular uncoupling may play a complex role in the initiation of reentry.

W-AM-D7

Effects of Sprint Training on Na^+/Ca^{++} Exchange Currents and SR Ca^{++} Contents of Rat Myocytes Following Myocardial Infarction

X.-Q. Zhang, T.I. Musch, and J.Y.Cheung Dept. of Med, Milton S. Hershey Med Cent, Pennsylvania State University., Hershey, PA 17033

We have previously shown that both Na^+/Ca^{++} exchange currents and SR Ca^{++} contents were lower in myocytes 3 week after myocardial infarction (MI). We have shown that high intensity sprint training (HIST) improved cardiac output in conscious instrumented MI rats. To explore cellular mechanisms of improvement in cardiac output by HIST, we measured skeletal muscle citrate synthase, myosin isoenzyme distribution in single cardiac myocytes, myocyte cell length, Na^+/Ca^{++} exchange currents, and SR Ca^{++} contents. 3 weeks after MI, rats were divided into sedentary (Sed; 10 m/min, 10 min/day, 0% grade, 5 d/week, n=20) and HIST (97 m/min, 15% grade, 5x1min bouts with 90 seconds rest between bouts, 5 d/week, n=19). Results obtained 9 weeks post-MI are: (*: $p<0.05$)

	Sed		HIST	
Cell length, um	130± 5	(24)	112±4	(22)*
Cell capacitance, pF	241.6±8.9	(44)	206.1±7.	(44)*
Citrate synthase,umol/g.min	22.1±2.8	(3)	23.2±2.7	(4)
Myosin, % α	55.3 ±0.3	(13)	88.6±2.6	(14)*
SR Ca^{++}, fmol/fF	5.3±0.6	(11)	7.6±0.7	(9) *

3-way ANOVA of repeated measures of I_{NaCa} at 1.8 mM and 5.0 mM $[Ca^{++}]_o$ indicated significant group (Sed vs. HIST, $p<0.0001$), voltage ($p<0.0001$), and $[Ca^{++}]_o$ ($p<0.0001$) main effects, and group x voltage x $[Ca^{++}]_o$ interaction ($p<0.0001$). We conclude that HIST may enhance cardiac performance after MI by: (1) attenuating myocytes hypertrophy; (2)restoring myosin isoform composition to normal; (3) improving Na^+/Ca^{++} exchange currents; and (4) increasing SR Ca^{++} contents.

W-AM-D8

Abstract Withdrawn.

W-AM-D9

INHIBITORY ACTION OF REPETITIVE STRETCH STIMULATION ON APOPTOSIS IN NEONATAL RAT CARDIOCYTES.

((**K. Yasui**, K. Kada and J. Toyama)) Dept. of Circulation, Res. Inst. Environ. Med., Nagoya University, Nagoya 464-01, Japan

We investigated the effect of repetitive stretch stimulation on apoptosis in cultured rat neonatal cardiocytes. Cardiac cells were cultured on elastic silicone dishes and were stretched by 20% in length repetitively at a frequency of 60 cycles/min during the second to third day of cultivation. To detect apoptosis, DNA fragmentation was assayed in situ by terminal deoxynucleotidyl transferase (TdT) mediated digoxigenin-dUTP nick-end labelling using peroxidase-based, direct immunocytochemistry. At day 2 of culture (before application of mechanical stretch), 1.9% of myocytes were stained positive by the nick-end labelling. In non-stretched myocytes, the percentage of stained myocytes progressively increased during culture (2.7% at day 4, 7.0 % at day 6 and 8.9% at day 8). Application of stretch stress for 24 hours at day 2 reduced occurrence of positively stained myocytes by the nick-end labelling (2.2% at day 6 and 4.2% at day 8). Our results suggest that mechanical stretch stress might play a role in survival of myocytes.

MEMBRANE FUSION: EXOCYTOSIS AND ENDOCYTOSIS II

W-AM-E1

TRIGGERED CALCIUM RELEASE FROM INTRATERMINAL STORES MAY PLAY A DIRECT ROLE IN NEUROPEPTIDE SECRETION: EVIDENCE FROM LIGHT SCATTERING IN MAMMALIAN NERVE TERMINALS. ((**B.M. Salzberg** and A.L. Obaid)) Dept. of Neuroscience, University of Pennsylvania School of Medicine, Phila. PA 19104.

Large and rapid changes in light scattering accompany secretion from mammalian neurohypophysial terminals (Salzberg et al., J. Gen. Physiol. 86: 395, 1985). These intrinsic optical signals are intimately related to the secretion of arginine vasopressin and oxytocin in mouse, but are absent in frog neurohypophysis. Interventions which modulate the amount of neuropeptide release (e.g., stimulation frequency; changes in $[Ca^{++}]_o$; D_2O substitution for H_2O) produce parallel changes in the amplitude of a component (S-wave) of the light scattering signal. This signal, that facilitates in a paired pulse protocol and is exhausted by high frequency stimulation, appears to follow the release of Ca^{++} from intraterminal stores in the mammal, triggered by the entry of Ca^{++} across the plasma membrane. Addition of caffeine (5 - 50 mM) to the bath results in a dramatic increase in the amplitude of the initial light scattering signal in a train, followed by a progressive diminution suggesting depletion of a small capacity compartment. This is consistent with caffeine's effect to increase the sensitivity of calcium-release channels to cytoplasmic Ca^{++}. TMB-8 [3,4,5-trimethoxy-benzoic acid-8-(diethylamino)octyl ester; 500 μM] nearly eliminates the S-wave of the intrinsic signal. Supported by USPHS grant NS 16824.

W-AM-E2

SINGLE VESICLE ANALYSIS OF MEMBRANE TRAFFIC IN RESTING CHROMAFFIN CELLS. ((**A. W. Henkel**, H. Meiri, M. Lindau and W. Almers)) Max-Planck-Institute for Medical Research, 69120 Heidelberg, Germany. (Spon. by L. Wollmuth)

Local changes in cell surface area were measured by monitoring the plasma membrane capacitance (C_m) of cell-attached patches with an 8 kHz sine wave. In quiet recordings, C_m steps of 0.1 fF could be reliably detected being 4 fold above the continuously monitored rms recording noise. A step increase indicated exo-, a decrease endocytosis. Endocytosis (frequency 9 mHz) moved twice more surface area than exocytosis (6 mHz; 76 cells). Histograms of endo- and exocytotic steps showed broad distributions between 0.2 and 4 fF. The endocytic histogram had, in addition, a sharp peak at 0.25 fF, corresponding to 90 nm dia vesicles. It may represent clathrin-coated vesicles since it disappeared after cytosolic acidification (n=56 cells). Acidified cells maintained normal membrane retrieval by an increased number of larger endocytic steps of broadly varying size. If the sharp endocytic peak represents clathrin-coated vesicles, <30 % of the surface and <4 % of the volume are internalized by this mechanism. A few cells (4 %) had many larger exocytic steps at 35-fold higher frequency. Some contain catecholamines (Albillos et al., this vol.). Their mean amplitude (1.3 fF) corresponds to 200 nm diameter vesicles since the average granule diameter in our cells is 330 nm. Raising cytosolic $[Ca^{2+}]$ by (i) depolarization, (ii) perfusion with ionomycin or (iii) flash photolysis of caged Ca failed to stimulate exocytic steps, even though in whole cell recordings (ii) and (iii) caused massive exocytosis translating into ten or more steps per patch. Evidently, cell-attached patches show no Ca triggered exocytosis while leaving constitutive traffic unimpaired.
Supported by SFB 317.

W-AM-E3

MOVEMENT, EXOCYTOSIS AND RESUPPLY OF SINGLE SECRETORY GRANULES SEEN BY EVANESCENT WAVE MICROSCOPY. ((**J.A. Steyer** and W. Almers)) Max-Planck-Inst. f. Med. Research, Heidelberg, Germany.

Secretory granules were fluorescently stained by incubating chromaffin cells with acridine orange and then removing the dye. Live cells adhering to the coverslip were viewed. With the evanescent wave (EW) of a totally reflected laser beam we selectively illuminated a 300 nm layer adjacent to the coverslip, exciting fluorescence in the granules located there. Fluorescent spots were readily seen, providing diffraction-limited images of single granules. Granules were remarkably stationary. In resting cells, they dithered around a fixed position with a diffusion coefficient of $D = 2.7 \pm 0.5 \cdot 10^{-11}$ cm^2/s (n=8, timescale of 100 ms) as if imprisoned in a cage 50 nm larger than a granule. Over minutes, also a slower motion was seen as if the "cage" itself diffused with $D = 9.7 \pm 1.6 \cdot 10^{-13}$ cm^2/s (n=10), or an r.m.s. speed of 1.2 μm/hr. When 62 mM external $[K^+]$ triggered Ca entry into cells, single granules disappeared abruptly (within one 0.6 s imaging interval). This represents exocytosis because (i) the loss of granules correlated with current spikes simultaneously recorded by a carbon fiber, and (ii) vanishing granules were often replaced for an instant by a visibly fluorescent cloud of secreted dye. Exocytosis often occurred locally, as if a "hot spot" of Ca influx depleted granules in a 2.0 ± 0.1 μm dia. circle (n=11). To study the recruitment of fresh granules to the plasmalemma, we allowed exocytosis during a 2 min exposure to high $[K^+]$, and counted the fluorescent spots at different times thereafter. Granules re-appeared with a time constant of 7±2 min (n=7). After settling beneath the plasmalemma, granules sometimes climbed back into the cytosol as if on an elevator, suggesting reversible docking. Some of them later descended at the same location back into the EW. Future studies will reveal the molecular mechanism of granule transport and docking.

W-AM-E4

RECONSTITUTION OF CALCIUM TRIGGERED EXOCYTOSIS *IN VITRO* USING 'RESERVE' GRANULES. ((S. S. Vogel, S. P. Radko, A. Chrambach & V. V. Chestkov)) SMS-NINDS, & LTPB-NICHD, NIH, Bethesda, MD 20892, and MGC-RAMS, Moscow, Russia.

Cells which secrete via triggered exocytosis typically contain both docked and reserve vesicles. While calcium dependent exocytosis has been studied in both intact and permeabilized cells, it is not known if pre-docked vesicles have different requirements for fusion than do reserve vesicles. Physiological experiments using intact and semi-intact systems suggest that ATP is not required for the final steps of calcium triggered exocytosis while biochemical analysis of the proteins thought to mediate vesicle docking involves intricate ATP dependent assembly processes. One way to resolve the ambiguity of the role of ATP in the final steps of calcium triggered secretion would be to determine whether granule docking requires ATP, or whether there is a requisite ATP dependent priming step subsequent to docking. In these cases reserve vesicles would require ATP for exocytosis while docked granules might not. To test this question, reserve exocytotic vesicles from sea urchin eggs were isolated by free-flow electrophoresis and used to reconstitute calcium triggered exocytosis. Reserve granules, like pre-docked cortical granules, do not require ATP for calcium triggered membrane fusion. ATPγS and GTPγS also did not inhibit membrane fusion. Thus, if there is a requisite ATP dependent step in secretion, such as the assembly or 'priming' of fusion complexes, this step must occur prior to vesicle docking. The data suggest that calcium triggered fusion of reserve exocytotic vesicles might be used to reseal plasma membrane lesions.

W-AM-E5

A REQUIREMENT FOR MgATP IN ENDOCYTOSIS AND POOL REFILLING, BUT NOT IN LATE STEPS OF EXOCYTOSIS
((**R. Heidelberger** and G. Matthews*)) MPI f. biophys. Chemie, Goettingen, Germany and *SUNY @ Stony Brook, Stony Brook, New York

The role of ATP in synaptic vesicle dynamics was investigated in synaptic terminals of goldfish retinal bipolar neurons. Whole-cell internal solution was supplemented with either (mM): 3 $MgCl_2$ and 2 Na_2ATP or 3 $MgCl_2$, 2 $Li_4ATP\gamma S$ and 0 Na_2ATP. The amplitude of the capacitance increase in response to the first voltage-step was similar under both conditions. The timecourse of endocytosis was at least 5-fold slower in the absence of ATP. A second depolarization given ~ 20 seconds after the first evoked a significantly smaller capacitance increase in the absence of ATP (20±13% of first, n=6), than with ATP (103±24% of first, n=13). Without ATP, recovery of the capacitance response was still incomplete when the second stimulus was given > 60 seconds after the first (54±11% of first, n=4). Examination of Ca-current, pre- and post-stimulation $[Ca]_i$, and time course of recovery of $[Ca]_i$ suggest that these effects are not mediated by differences in Ca-influx or $[Ca]_i$. Flash-photolysis studies with caged-Ca revealed no obvious difference in release kinetics when internal solution contained MgATP, $MgATP\gamma S$ or 0 ATP. These results suggest that ATP has little effect on the fusion kinetics of the readily-releasable pool of synaptic vesicles, but it is important for membrane retrieval and refilling of the readily-releasable pool.

W-AM-E6

DYNAMIN-1 REGULATION OF RAPID ENDOCYTOSIS IN ADRENAL CHROMAFFIN CELLS INVOLVES THE PH DOMAIN.
((**C. R. Artalejo**[1], M. A. Lemmon[2], J. Schlessinger[2] and H. C. Palfrey[3])). [1]Dept. Pharmacol., Wayne State Univ. Med. School, Detroit, MI 48201; [2]Dept. Pharmacol., NYU Med.Center, NY, NY 10016; [3]Dept. Pharmacol. & Physiol. Sci., Univ. Chicago, Chicago, IL 60637.

Rapid endocytosis (RE), the principal mechanism whereby calf adrenal chromaffin (AC) cells recover vesicular membrane after exocytosis, depends on GTP hydrolysis and the GTPase dynamin but does not involve clathrin (Artalejo et al, PNAS 92, 8328, 1995). All dynamins contain a central pleckstrin homology domain (PHd) whose role is obscure. Introduction of the bacterially-produced PHd from dynamin-1 (0.5 mg/ml) into the cells via a patch pipette completely inhibited RE as measured by cell membrane capacitance. This effect was specific as the PHds of dynamin-2, PLCδ1 or pleckstrin had no effect on RE. PCR, RNA blot and immunoblot analysis revealed that AC cells express both dynamin-1 and dynamin-2. The PHd's of dynamin-1 and -2 are 81% identical. To ascertain which amino acids were responsible for the specific effect of the dynamin-1 PHd we constructed chimeric proteins guided by the crystal structure of this domain (Ferguson et al, Cell 79, 199, 1994). Substitution of just 2 amino acids in a variable loop between β-strands 1 and 2 in the dynamin-2 PHd with the corresponding amino acids from dynamin-1 (SL->GI) produced a gain-of-function dynamin-2 mutant whose recombinant protein was fully inhibitory to RE. These results indicate that the PH domain of dynamin-1 is critical to its endocytotic function and suggest that dynamins-1 and -2 may interact specifically with different membrane sites and possibly regulate distinct forms of endocytosis (Supported by NIH and Sugen).

W-AM-E7

RAPID ENDOCYTOSIS HAS NO ABSOLUTE DEPENDENCE ON CALCIUM
((**Paolo G.P. Nucifora** and Aaron Fox)) Dept of Pharmacological and Physiological Sciences, The University of Chicago, 947 E. 58th Street, Chicago, Illinois, 60637. (Spon. by A. Harkins)

Catecholamine secretion in bovine adrenal chromaffin cells can be triggered by calcium, strontium, or barium influx. Rapid endocytosis is less well defined. Some studies have proposed that calcium does not trigger rapid endocytosis, while other studies have documented a strict calcium dependency. In one study, the activation of calmodulin was required for rapid endocytosis. Our data show that rapid endocytosis can proceed normally when secretion is triggered by barium rather than calcium, which indicates that there is no absolute requirement for calcium. In initial stimulations, neither the rate of retrieval nor retrieval quantities were diminished when barium was substituted for calcium in the extracellular solution. However, in subsequent stimuli, the replacement of calcium with barium did produce kinetic differences in endocytosis, suggesting the possibility of a long-term role for calcium. These results also imply that calmodulin activation is not a prerequisite for rapid endocytosis, as barium is not thought to activate calmodulin. In support of this conclusion, we did not detect an effect on endocytosis when calmidazolium, a potent calmodulin antagonist, was dialyzed into cells at concentrations as high as 1 μM. While the role of calcium in eliciting rapid endocytosis is still not well understood, these findings demonstrate either that there is no requirement for calcium in endocytosis or that barium can act as a substitute in the final steps of this process.

COLICINS: STRUCTURE, FUNCTION, EVOLUTION

W-AM-F1

THE CRYSTAL STRUCTURE OF COLICIN IA.
((**M.C. Wiener***, D.M. Freymann, P. Williams, P. Ghosh†, R.M. Stroud)) Dept. of Biochemistry & Biophysics, University of California, San Francisco, 94143-0448, *Dept. of Molecular Physiology & Biological Physics, University of Virginia Health Sciences Center, 22906-0011, †Dept. of Molecular & Cellular Biology, Harvard University, 02138.

The formation of ion-permeable channels in target cell membranes is a general mechanism of cytotoxicity. The process involves secretion of a soluble protein which inserts into the plasma membrane of the target cell and forms a lethal pore. Colicins, *Escherichia coli* protein toxins, are a well-characterized example of this class of proteins. Colicin Ia crystals, comprised of approximately 80% solvent, are in spacegroup $C222_1$ (a=64.4Å, b=178.6Å, c=285.5Å). All data sets used in the structure determination were collected from frozen crystals with a synchrotron light source (SSRL beamline 7-1). Heavy atom derivatives were obtained using mercurial soaks of engineered single-site cysteine mutants. The crystal structure of the 69kD colicin Ia protein reveals the structures of the three distinct domains which function, respectively, to i) bind to a receptor on the outer membrane of susceptible bacteria, ii) translocate across the outer membrane, and iii) bind to the inner membrane and form a pore in the presence of the transmembrane voltage. The domains are separated by an extraordinarily long helical coiled-coil. Colicin Ia and other group B colicins enter susceptible cells by hijacking the bacterial tonB translocation pathway. The specific location of the conserved tonB box in the translocation domain of colicin Ia, and the structural relationship between the three domains, suggest possible mechanisms for colicin uptake.

W-AM-F2

STRUCTURE-FUNCTION RELATIONSHIPS IN THE CHANNEL-FORMING DOMAIN OF COLICIN E1.
((**P. Elkins**, A. Bunker, W.A. Cramer and C.V. Stauffacher)) Department of Biological Sciences, Purdue University, West Lafayette, IN 47907.

Colicin E1 is a bacteriocin whose toxic action is expressed in the formation of a voltage-gated channel in the inner membrane of a target *E. cell*. A substantial structural conversion is necessary for this protein to go from a soluble toxin to a membrane-channel state. One can gain a number of insights into this structural rearrangement from examining the structure of the C-terminal channel-forming domain of colicin E1, recently solved at 2.5Å resolution. The structure of the channel-forming domain of colicin E1 is a sandwich of helices arranged in three layers, with the central layer a hydrophobic hairpin believed to be important in the anchoring of the channel domain to the membrane. The two outer layers are composed of amphipathic helices, which are proposed to open out onto the membrane surface in the closed channel state of the molecule. The pathway of structural unfolding between these events is suggested by several distinctive features of the colicin E1 structure. The distribution and conservation of positively charged residues on the molecule's surface suggests an orientation for the first step of membrane attachment, which is dependent on electrostatic interaction with the anionic membrane surface. Interior cavities between helical layers suggest a pathway by which the structure unfolds on the membrane surface after initial attachment. Flexible helical domains and helical movements relative to the other channel-forming colicin structures indicate helical rearrangements which may accompany the conversion of colicin E1 to a membrane-attached protein.

W-AM-F3

CRYSTAL STRUCTURE OF COLICIN E3 IMMUNITY PROTEIN.

((D. Zhao, A. Zappala, A. Djebli and **M. Shoham**))
Case Western Reserve University School of Medicine, Department of Biochemistry, Cleveland, Ohio 44106-4935.

Colicin E3 is a cytotoxin that functions enzymatically. It nicks 16S rRNA at a specific site, thereby blocking protein biosynthesis in the infected cell. The immunity protein acts as a specific inhibitor of this RNase function by forming a 1:1 complex with colicin E3. The crystal structure of an immunity protein dimer has been solved at 1.9Å by MIR phasing. The secondary structure of the monomer consists of a four-stranded antiparallel β-sheet and a short α-helix. Cocrystals of colicin E3 and its immunity protein diffract to 2.8Å resolution. They belong to the monoclinic space group $P2_1$ with unit cell dimensions a=68.6, b=193.7, c=84.5Å and β=113.1°, and four molecules of the complex per asymmetric unit. The structure determination is in progress by MIR phasing and non-crystallographic symmetry averaging.

W-AM-F4

Energetics of colicin uptake and immunity

Holger Pilsl and Volkmar Braun, Microbiology / Membrane-physiology, University of Tübingen, 72076 Tübingen, Germany

Pore-forming colicins dissipate the electrochemical potential of the cytoplasmic membrane and kill cells. Sensitive cells import group B colicins via an energy-consuming process across the outer membrane in which no energy source exists. It is the electrochemical potential of the cytoplasmic membrane that energizes transport across the outer membrane. The energy-transducing device consists of three proteins named TonB, ExbB, and ExbD. A similar device, named TolA, TolQ, TolR and TolB exists for the uptake of group A colicins. New data on the conversion of a Tol-dependent colicin into a Ton-dependent colicin, and studies on the interaction of immunity proteins with colicins in the cytoplasmic membrane are relevant for the understanding of how colicins are translocated across the outer membrane and inserted into the cytoplasmic membrane.

W-AM-F5

STOPPED-FLOW FLUORESCENCE ANALYSIS OF THE KINETICS FOR THE FOLDING MECHANISM OF THE COLICIN E1 CHANNEL PEPTIDE. ((B.A. Steer and A.R. Merrill)) Guelph-Waterloo Centre for Grad. Work in Chem., Dept. of Chem. & Biochem., Univ. of Guelph, Guelph, ON, CAN, N1G 2W1.

The equilibrium unfolding pathway of the colicin E1 channel peptide was shown in a previous study to involve an unfolding intermediate, stable in approximately 4 M guanidine hydrochloride, which comprised primarily the C-terminal hydrophobic α-helical hairpin segment of the peptide. In this study, the structural nature of this unfolding intermediate was investigated further and it was found that the intermediate is dimeric and comprised of two partially denatured monomeric peptides, which appear to be associated by hydrophobic interactions. The dimerized structure was detected by size-exclusion high performance liquid chromatography, sodium dodecyl sulphate polyacrylamide electrophoresis and intermolecular fluorescence energy transfer. Using stopped-flow fluorescence spectroscopy, the kinetics of the denaturation and dimerization of the colicin E1 channel peptide in 4 M guanidine hydrochloride were examined. Denaturation kinetics were also investigated by wild-type peptide Trp fluorescence and 1-anilinonaphthalene-8-sulfonic acid binding. The kinetics of dimer formation were examined by monitoring the time dependence of intermolecular Trp to 5-[[[[iodoacetyl]amino]ethyl]amino]-naphthalene-1-sulfonic acid fluorescence resonance energy transfer upon denaturation in 4 M guanidine hydrochloride. In addition, single Trp mutant peptides were employed as site-specific fluorescent probes of unfolding kinetics and reported diverse and characteristic unfolding kinetics. However, it was shown that following a rapid and major unfolding transition the peptide's core residues cluster slowly, by hydrophobic association, forming an intermediate species which is a prerequisite to dimerization. These equilibrium and kinetic unfolding data describe an unique unfolding mechanism where the channel peptide forms a partially unfolded dimerized structure in 4 M guanidine hydrochloride [supported by NSERC, ARM].

W-AM-F6

DETERMINATION OF MEMBRANE-PROTEIN TOPOLOGY BY RED-EDGE EXCITATION SHIFT ANALYSIS. ((M.C. Tory and A.R. Merrill) Guelph-Waterloo Centre for Graduate Work in Chemistry, Dept. of Chemistry and Biochemistry, University of Guelph, Guelph, ON, Canada, N1G 2W1.

Under acidic conditions, colicin E1 (or colicin E1 channel peptide) inserts into membrane bilayers, forming a voltage-gated ion channel. *In vivo*, formation of the channel within the cytoplasmic membrane is sufficient to effect lethal cell depolarization. The mobility of the tryptophan residue(s) of wild type and 15 single Trp mutant colicin E1 thermolytic channel peptides in both the soluble and membrane-associated state was investigated using red-edge excitation analysis. A dependence of (*i*) the wavelength of maximum fluorescence emission and (*ii*) the fluorescence anisotropy of the mutant proteins on the excitation wavelength was observed for most of the single Trp mutants, in both the soluble and membrane-associated state. In most cases, the dependence was manifested as a red-edge excitation shift (REES), suggesting the residues are located within a motionally-restricted environment. Excitation wavelength dependence was not observed for the Trp residue at position 443 in either the membrane-associated or soluble state. The Trp residue at position 355 also did not exhibit REES in the membrane-associated state, however, it did show a blue shift in the soluble peptide. Comparison of the extent of REES measured for the Trp residue of each mutant protein will provide site-specific insight into the degree of motional-restriction within different regions of the channel peptide. This information can be combined with other data to map the topology of the colicin E1 channel peptide within the membrane bilayer. [Supported by NSERC, ARM]

W-AM-F7

A FOREIGN EPITOPE IS TRANSLOCATED ACROSS LIPID BILAYERS IN ASSOCIATION WITH GATING OF COLICIN Ia CHANNELS ((K. Jakes, P. Kienker, S. Slatin, and A. Finkelstein)) Albert Einstein College of Medicine, Bronx, NY 10461

Channel-forming colicins are bactericidal proteins that make voltage-dependent channels in the inner membrane of susceptible cells and in planar lipid bilayers. We have previously shown that gating of the channel is associated with the movement of about 70 amino acids of the channel-forming domain back and forth across the membrane. We report here on the insertion of foreign protein into the translocated segment of colicin Ia. The nine amino acid HA epitope of influenza virus hemagglutinin protein was inserted, by site-directed mutagenesis, between helices 3 and 4 of the channel-forming domain of colicin Ia. The resultant colicin protein has significant bactericidal activity and it makes voltage-dependent channels in planar lipid bilayers. A monoclonal antibody directed against the HA epitope blocks turn-off of the channels when added to the *trans* compartment, indicating that this foreign peptide is translocated across the bilayer in conjunction with channel opening. The effect of the antibody is specifically blocked by prior addition of the nine amino acid HA peptide to the *trans* compartment. The colicin Ia channel is thus capable of translocating at least nine amino acids of foreign protein across the membrane during gating.

W-AM-F8

STRUCTURAL ANALYSIS OF THE MEMBRANE-BOUND STATE OF THE C-TERMINAL CHANNEL DOMAIN OF COLICIN E1 AND A HYDROPHOBIC HAIRPIN EXTENDED MUTANT ((M. Lindeberg and W. A. Cramer)) Dept. of Biol. Sci., Purdue Univ., West Lafayette, IN 47907. (Spon. by S. E. Ostroy)

To better characterize the orientation of the hydrophobic hairpin in the membrane-bound ColE1 channel domain, the mutant ColE1-hhx was created by insertion of an 8-residue, tryptophan-containing extension at the tip of the hydrophobic hairpin. When wild-type 178 residue channel domain was bound to liposomes encapsulating the quenchers I^- or IO_3^-, no quenching of Trp fluorescence was observed. However, with the ColE1-hhx channel domain, fluorescence was significantly quenched by 0.15 M IO_3^-, with a $t_{1/2} = 28 \pm 3$ sec at 25° following addition of liposomes [DOPG:DOPC (40:60)] to free channel polypeptide. In contrast, no quenching by I^- was seen. To assess the cause of differential quenching by the two ions, wild-type and ColE1-hhx channel domain were bound to liposomes in the presence of external IO_3^- and I^-. Quenching of Trp fluorescence by external IO_3^- was 25-30% greater than by external I^-, suggesting that IO_3^- penetrates further into the interfacial layer. It is hypothesized that the additional residues in ColE1-hhx stabilize the tip of the hydrophobic hairpin near the interfacial layer of the *trans* side of the bilayer, resulting in quenching of one or more Trp by IO_3^- in the interfacial layer. In contrast, wild-type ColE1 channel domain is quenched by neither encapsulated IO_3^- or I^-, suggesting that the native hydrophobic hairpin is either too short or too mobile to exhibit quenching by IO_3^-. Differential quenching patterns of membrane-bound single Trp mutants of ColE1 channel domain by externally added IO_3^- indicate that IO_3^- may be a useful probe for distinguishing small differences in the extent of insertion of Trp residues of membrane-active proteins into the membrane interfacial layer. (NIH GM-18457).

W-AM-F9

STRUCTURE ANALYSIS OF THE C-TERMINAL CHANNEL DOMAIN OF COLICIN E1 IN ITS SOLUTION AND MEMBRANE-BOUND STATES. ((S. D. Zakharov[1], S. Yu. Venyaminov[2], F. G. Prendergast[2], and W. A. Cramer[1])) Dept. of Biol. Sci., Purdue Univ., W. Lafayette, IN 47907[1]; Dept. Pharmacol., Mayo Foundation, Rochester, MN 55905[2]. (Spon. by W. L. Pak)

The structure of the colicin E1 channel domain and its melting in the water-soluble and membrane-bound states were analyzed by circular dichroism in the far and near UV, and infra-red spectroscopy. The content of α-helical (ordered and distorted), β-sheet (ordered and distorted), β-turn, and unordered structures could be determined. A significant increase (ca. 30%) of the ordered α-helical structure in the membrane-bound state was accompanied by a decrease (ca. 25%) in unordered structure. The change in content of distorted α-helical structure and in the number of α-helical segments was insignificant (10 segments in the membrane-bound state). The average length of α-helical segments in the water-soluble and membrane-bound states was 13 and 18 residues, respectively, implying that several α-helical segments in the colicin E1 channel domain are long enough to traverse the membrane bilayer. Membrane binding is accompanied by an almost complete loss of amplitude of the near-UV CD spectrum.

A significant difference in the melting of channel domain structure in solution and in the membrane-bound state was observed by far and near UV CD. The protein melting in solution is highly cooperative with a transition midpoint at 57° and half-width < 8°. Unfolding in solution is followed by the formation of intermolecular β-structure. Protein stability is ionic strength-dependent. The melting of the membrane-bound protein is non-cooperative (a broad peak with half-width 30-40° at 50°) and completely reversible. [Supported by NIH GM18457 (WAC) and GM34847 (FGP)]

EPITHELIAL PHYSIOLOGY

W-AM-G1

THE ROLE OF LENS MIP IN THE TRANSPORT AND METABOLISM OF GLYCEROL ((C.Kushmerick, K. Varadaraj and R.T. Mathias)) Dept. Physiology and Biophysics, SUNY Stony Brook, NY 11794.

Lens MIP is the most abundant protein of the fiber cell membrane. We have recently shown that, expressed in Xenopus oocytes, MIP formed a water channel, facilitated glycerol uptake and appeared to stimulate glycerol metabolism (Kushmerick et al, Exp. Eye. Res. 61:351-62 1995). In the present study, we examined the effects of MIP on glycerol uptake and metabolism. Glycerol permeability (P_{Gly}) was 2.3±0.23 x 10^{-6} cm s^{-1} with MIP vs. 0.92±0.086 x 10^{-6} cm s^{-1} in control oocytes. The component of P_{Gly} due to MIP was independent of concentration from $5x10^{-5}$ to $5x10^{-2}$ M and had a low temperature dependence, suggesting permeation through MIP occurs by diffusion in a water-filled pore, rather than via a carrier mechanism. The pharmacology of MIP was similar to other glycerol transporters; P_{Gly} of MIP was inhibited approximately 90%, 80% and 50% by 1.0 mM Hg^{++}, 0.2 mM DIDS, and 0.1 mM Cu^{++}, respectively. Expression of MIP also stimulated glycerol phosphorylation. We measured the activity of glycerol kinase as a function of free intracellular glycerol. The apparent dissociation constant of the kinase was ≈12 μM and was unchanged by expression of MIP whereas turn-over was significantly increased (0.12±0.03 vs. 0.06±0.01 pmol min^{-1} $cell^{-1}$). We therefore conclude that expression of MIP either allosterically increased turn-over per kinase or induced expression of more kinase. We incubated intact frog lenses in the presence of ^{3}H-glycerol and recovered ^{3}H-glycerol-3-phosphate from the fiber cells. Thus lens fiber cells are capable of taking up and metabolizing glycerol, and MIP may participate in this process. Supported by the NIH NEI EY06391.

W-AM-G2

DUAL ROLE OF PROSTAGLANDIN E_2 IN REGULATION OF Na^+ TRANSPORT IN A6 EPITHELIA. ((T. G. Paunescu and S. I. Helman)) Department of Molecular & Integrative Physiology, University of Illinois at Urbana-Champaign, Urbana, IL 61801.

A pulse method of blocker-induced noise analysis was used to study the time-dependent changes of channel density (N_T), open probability (P_o) and single-channel current (i_{Na}) of Na^+ channels in A6 epithelia in response to 1μM PGE_2 added to the basolateral solution for 2 hours. Epithelia derived from two different cell passages (p73 and p109) were investigated in both non-stimulated and aldosterone-stimulated conditions (n=4 for each of 4 groups). The macroscopic short-circuit current ($I_{Na} = i_{Na} \cdot P_o \cdot N_T$) was stimulated in all tissues due to large increases of N_T, but with relatively large compensatory decreases of P_o. I_{Na} reached peak values within 15 min and its increase was baseline-dependent. I_{Na} increased from 4.3±1.3 to 9.4±1.1 μA/cm^2 in p73 non-stimulated tissues, while in p109 aldosterone-pretreated tissues, I_{Na} increased from 20.9±1.5 to 30.4±2.9 μA/cm^2. Regardless of baseline, N_T increased to peak values 3.7 to 5.6 times above respective controls occurring more rapidly in aldosterone-pretreated tissues. Maximal decreases of P_o were observed within 5 min in aldosterone-pretreated tissues; 0.24±0.03 to 0.06±0.02 (p109) and 0.23±0.06 to 0.08±0.03 (p73). From peak values, both N_T and P_o returned towards but remained changed from control for the duration of the experiments. (Supported by NIH DK 30824 and UIUC Campus Research Board)

W-AM-G3

FUNCTIONAL CHARACTERIZATION OF APX, A NOVEL RENAL EPITHELIAL Na^+ CHANNEL. ((A.G. Prat[1], E.J. Holtzman[1], D. Brown[1], C.C. Cunningham[2*], I.L. Reisin[3*], T.R. Kleyman[4], G.R. Jackson Jr.[1*], and H.F. Cantiello[1])) 1. Renal Unit, Mass. Gen. Hosp. East, Charlestown, MA, USA; 2. Exp. Med., Brigham and Women's Hosp., Boston, MA, USA; 3. Cátedra de Química Gen. e Inorgánica, Fac. de Farmacia y Bioquímica, Buenos Aires, Argentina; 4. Depts. of Med. and Physiol., Univ. of Pennsylvania & VA Med. Ctr, Philadelphia, PA, USA

Apx is a recently cloned amphibian protein which, although associated with renal amiloride-sensitive Na^+ channel activity, has previously failed to generate amiloride-sensitive Na^+ currents (Staub et al., JCB 119: 1497, 1992). Thus, based on the hypothesis that Apx-mediated channel activity may be tonically inhibited by the actin cytoskeleton, Apx was expressed in human melanoma cells with a defective actin-based cytoskeleton. Membrane-associated Apx expression was linearly correlated with a 60-900% increase in amiloride-sensitive (K_i = 3 μM) Na^+ currents of various clones. Single channel Na^+ currents of clone Apx-7 were observed under spontaneous conditions, or were induced by addition of either actin- or PKA plus ATP. Na^+ channels had a similar functional fingerprint to the vasopressin-sensitive (Prat et al., AJP 265:C218, 1993), and actin-regulated epithelial Na^+ channel of A6 cells (Cantiello et al., AJP 261:C882, 1991; Prat et al., AJP 265:C224, 1993), including a 6-7 pS conductance and a 4:1 Na^+:K^+ perm-selectivity. Membrane-enriched fractions from Apx-7 cells were also reconstituted into lipid bilayers to assess for Na^+ channel activity. Either spontaneous or actin-induced ion channel activity was observed in symmetrical 150 and 300 mM NaCl. Reconstituted channels had a single channel conductance of 11-15 pS (n=4) in symmetrical 150 mM NaCl, rectified in a cation-selective manner, displayed a Na^+:K^+ perm-selectivity value of 4-6:1, and were inhibited by addition of *trans* amiloride (1 μM). Membrane-preparations from non-transfected cells showed no channel activity (n=4). Apx has properties consistent with the pore-forming 150 kDa subunit of an epithelial Na^+ channel complex initially purified by Benos (Benos et al., JBC 262:10613, 1987). Apx may be responsible for the ionic conductance involved in the vasopressin-activated Na^+ reabsorption in the amphibian kidney.

W-AM-G4

THE EFFECT OF pH ON THE KINETICS OF THE PROXIMAL TUBULAR Na-HCO_3 COTRANSPORTER.

((Eltan Gross and Ulrich Hopfer)) Dept. of Physiology & Biophysics, Case Western Reserve University, 10900 Euclid Ave, Cleveland, OH 44106-4970.

The principal pathway for uphill movement of acid from cell to tubular fluid, in the proximal tubule, is via the luminal Na/H exchanger. The major transport pathway for HCO_3 exit across the basolateral membrane is the electrogenic Na-HCO_3 cotransporter. The requirement of intracellular salt- and pH-homeostasis, under conditions of high through fluxes calls for a high degree of coordination between the activities of these transporters. One possible mechanism which enables this "cross-talk" between the two transporters is regulation by intracellular pH. We studied the effect of pH on the K_m for Na of the cotransporter in an immortalized rat proximal tubular cell line. Cells were grow on a permeable support and electrophysiology experiments were carried out in a Ussing chamber. Cell monolayers were permeabilized with luminal amphotericin B and voltage-current relations were measured in absence and presence of basolateral DNDS (a reversible inhibitor of the cotransporter) at different Na concentrations. The DNDS-sensitive current vs. voltage (I-V) relation at each [Na] was fitted to a straight line from which cotransporter's conductance was calculated. K_m values for Na were obtained from the DNDS-sensitive conductance versus [Na] data. To study the effect of pH on K_m, the solutions were buffered with HEPES and the pH was set to either 7.5 or 7.0. To maintain a constant [HCO_3] of 18 mM, solutions were pre-equilibrated at either 3% or 10% CO_2 atmospheres, respectively. The K_m for Na increased from 3.6 mM at pH 7.5 to 5.5 mM at pH 7.0. These data suggest that changes in intracellular pH may play an important role in regulating the Na-HCO_3 cotransporter activity in the proximal tubule, such that a lower cytosolic pH decreases Na-HCO3 cotransporter activity. (NIH grant HL41618).

W-AM-G5

THREE K^+ CHANNELS IN PORCINE GRANULOSA CELLS: A ROLE IN STEROIDOGENESIS? ((**DE Mason**, JJ Lippold, GA Herin, JL Baranao*, LC Freeman)) Kansas State University, Manhattan, KS & IBYME*, Buenos Aires, Argentina (Spon: RF Gilmour, Jr.)

Using whole cell patch clamp in porcine granulosa cells (PGC), we have identified three K^+ currents: a slowly activating, non-inactivating delayed rectifier; a rapidly activating, inactivating transient outward K^+ current; and an ultra-rapidly activating delayed rectifier. Using RT-PCR or immunofluorescence we have identified the molecular correlates of these currents. We have shown that the slow delayed K^+ current is a minK channel protein (*Biophys J* 70: A312, 1996). This minK current is present in PGC acutely isolated from ovarian follicles, but not in cultured PGC, nor passaged primary cultures. We have also demonstrated minK current and message in bovine granulosa cells (BGC), and in an immortalized line from undifferentiated BGC (BGC-1). The ultra-rapidly activating delayed rectifier, which kinetically resembles Kv1.5, is present in acutely isolated and cultured PGC, where positive immunostaining can be demonstrated using Kv1.5 specific antibody. The rapidly activating, inactivating K^+ current is present only in differentiated passaged primary PGC which show positive immunostaining using Kv1.3 specific antibody. Treatment of PGC cultures to K^+ channel antagonists suggests that one or more of these channels may be involved in PGC growth and differentiation. Clofilium (25 μM) and verapamil (100 μM) inhibit progesterone accumulation in the media of monolayer PGC cultures, days 1 - 4 and decreases the viable cell count on day 4 of culture. Charybdotoxin (10 nM) and 4-AP (1-2 mM) have no effect on progesterone accumulation or cell counts during days 1 - 4 of culture. These findings suggest that expression of K^+ channel proteins changes during granulosa cell growth differentiation, and that K^+ channels may play a role in steroidogenesis in granulosa cells.

W-AM-G6

FUNCTIONAL MODIFICATION OF AN EPITHELIAL CHLORIDE CHANNEL BY CHEMICAL REAGENTS. ((**M. Duszyk** and S.F.P. Man)) Departments of Physiology and Medicine, University of Alberta, Edmonton, Alberta T6G 2H7, Canada

Chemical modification of ion channels can give important information about the specific essential structures involved in their function. In this study, we characterized the effects of different group-specific reagents on the function of Cl^- channel from bovine tracheal epithelium. Apical membrane proteins were incorporated either into giant liposomes suitable for patch clamp studies, or into liposomes loaded with Cl^--sensitive fluorophore 6-methoxy-N-[3-sulfopropyl] quinolinium (SPQ), for Cl^- influx studies. Giant liposomes were formed from L-α-lecithin by a dehydration-hydration method and ion channels were characterized using the excised inside-out configuration. Liposomes for Cl^- influx studies were formed using gel filtration on Sephadex G-50-80. A number of site-specific reagents were investigated and their effects on ion channel function were characterized using the above methods. Modification of amino groups using trinitrobenzene-1-sulfonic acid or methyl acetimidate reduced Cl^- flux and single channel open probability. On the other hand, N-bromoacetamide that modifies proteins at the carboxyl end of cysteine, histidine, phenylalanine, tyrosine and tryptophan residues increased Cl^- flux. Modification of arginine residues had no effect on channel function. These results suggest that several amino acid residues are involved in control of gating of an epithelial Cl^- channel.

W-AM-G7

IDENTIFICATION OF THE H^+ SENSOR OF ClC-2G(2α) Cl^- CHANNELS. ((**K. Stroffekova**, E. Kupert, D.H. Malinowska and J. Cuppoletti)) UC Coll Med, M&C Physiol, Cincinnati, OH 45267-0576.

ClC-2G(2α) Cl^- channel is PKA and H^+ activated (Malinowska, *et al* AJP 268 Cell Physiol 37:C191-C200, 1995). It differs from the rat voltage- and volume-regulated ClC-2 Cl^- channel in showing both pH and PKA activation. The present study was to identify the H^+ sensor of rabbit ClC-2G(2α). When pH was asymmetrically reduced from pH 7.4 to 3.0 in the *trans* compartment, corresponding to the outer face of the channel, Po at -80 mV significantly ($P<0.001$) increased by 4 fold from 0.20 ± 0.03,n=5,N=3 to 0.80 ± 0.07,n=7,N=4. A Hill plot of the H^+ activation profile was linear over the range of pH 3 to 7.4, with an $n\leq1$ and an EC_{50} at pH 4.7. Thus, a single or non-interacting acidic residue(s) is likely responsible for pH activation. Only one acidic residue on the outer face of the channel, E419, differs between rabbit ClC-2G(2α) and rat ClC-2. Mutagenesis of E419 to G, as found in rat ClC-2, yielded a channel with a Po which was significantly greater ($P<0.001$) than the wild type channel at pH*trans* 7.4 and -80 mV ($Po=0.59\pm0.04$,n=21,N=8). Closed times were dramatically decreased. No other effects of modification were observed. Glycine methyl ester modification of carboxyl groups of ClC-2G(2α) catalyzed by the water soluble carbodiimide, 1-ethyl 3(3-dimethylaminopropyl)carbodiimide, (EDC), gave similar extents of activation to 0.56 ± 0.07, increasing apparent NPo and decreasing closed times at -80mV. Similar effects were observed at +80 mV with all treatments. These results demonstrate that acidic residue(s) on the outer face of the channel regulate Po and identify E419 as essential in H^+ activation of ClC-2G(2α). Supported by NIH DK431816, DK433377 and CFFR457.

MOLECULAR RECOGNITION ON THE MEMBRANE SURFACE: MEMBRANE TARGETS AND BINDING MOTIFS

W-AM-SymII-1 **D. Kendall, University of Connecticut**
Signal Peptide Charge and Hydrophobicity: Requirements for Recognition During Membrane Translocation

W-AM-SymII-2 **A. Newton, University of California, San Diego**
Regulation of Protein Kinase C's Membrane Interaction by Two Membrane-Targeting Domains

W-AM-SymII-3 **S. Scarlata, SUNY at Stony Brook**
Role of Pleckstrin Homology Domains in Phospholipase C Activation: Two Distinct Binding Targets by a Single Motif

W-AM-SymII-4 **S. Sprang, HHMI, University of Texas SW Medical Center**
C2 Domains

W-AM-H1

COMPLEMENTATION OF VOLTAGE SENSOR MUTATIONS BY MUTATIONS IN THE PORE OF DRK1. ((M.L. Chapman, H.M.A. VanDongen, A.M.J. VanDongen)) Dept of Pharmacology, Duke University Medical Center, Durham, NC 27707.

The potassium channel voltage sensor is comprised of a series of basic amino acids in the fourth transmembrane segment (S4) in conjunction with acidic residues in the second and third transmembrane segments (S2 and S3). We have constructed mutants in both components of the voltage sensor which resulted in depolarizing shifts in the half-activation voltage ($V_{1/2}$) by as much as 70 mV. Introduction of these mutations into a pore variant of drk1 (drk1-L) abrogated the shifts in $V_{1/2}$, though the midpoint of drk1-L was not different from that of drk1. Analysis of activation and deactivation kinetics suggested that the open state was stabilized in drk1-L and that the voltage sensor mutations diminished this stability. These data are consistent with a multistate model in which voltage-dependent activation and voltage-independent channel opening are distinct, yet coupled, processes. In this context, the enhanced open state stability of drk1-L can be attributed to an increase in the voltage-independent forward rate constant of channel opening. Additionally, the depolarizing shifts caused by the voltage sensor mutations must be due to increases in the voltage-dependent reverse rate constant of the final step in activation.

W-AM-H2

AN EXTERNAL POTASSIUM BINDING SITE REVEALED IN DRK1, A VOLTAGE-GATED K CHANNEL. ((H.S. Krovetz, H.M.A. VanDongen, and A.M.J. VanDongen)) Dept. of Pharmacology, Duke University Medical Center, Durham, NC 27707.

The pore of an ion channel is comprised of a narrow region defining ion selectivity and permeation flanked by widening internal and external vestibules. We used divalent cations to probe the surface accessibility of cysteine substituted mutants in the pore region of the drk1 channel. At two introduced metal binding sites, I379C and Y380C, the binding of cadmium was relieved by increasing amounts of external potassium. The ability of external potassium to relieve cadmium block depended critically upon the Debye length indicating an electrostatic interaction between the potassium and cadmium binding sites. Binding of ions at this site is voltage-independent even though this site has the basic selectivity profile of the drk1 channel (K^+>Rb^+>>Na^+>Li^+). Mutations in the deep pore that alter the K^+:Rb^+ selectivity of the channel also affect the apparent affinities of this site for K^+ and Rb^+. These data suggest that this monovalent cation binding site is part of the permeation pathway of the channel. Thus it appears that a component of the selectivity filter of drk1 is exposed to the external environment of the channel and is outside of the membrane electric field.

W-AM-H3

REGULATION OF ION-DEPENDENT GATING AND BLOCK BY CONSERVED AROMATIC AMINO ACID RESIDUES IN THE PORE OF VOLTAGE-GATED K^+ CHANNELS. ((Glenn E. Kirsch and Char-Chang Shieh)). Department of Physiology and Biophysics, Case Western Reserve University, Rammelkamp Center, MetroHealth campus, Cleveland OH 44109.

The P-region of voltage-gated K channels contains a highly conserved triplet of aromatic residues (Phe^{433}-Trp^{434}-Trp^{435}, *Shaker*). Trp^{434}→Phe substitution produces a non-conducting *Shaker* K channel that gates normally, but the mechanism and generality of this effect are unknown. We have mutated the corresponding residues (364-366) in Kv2.1 to either Tyr or Phe. When expressed in *Xenopus* oocytes, W365F (corresponding to *Shaker* W434F), produced robust ionic currents with slightly enhanced inactivation and a 30-fold decrease in external TEA block. By contrast, Tyr substitution (W365Y) caused markedly accelerated inactivation gating, K-dependent ion conduction and a five-fold reduction in TEA block. Ionic currents were abolished by removal of external permeant ions. Tyr substitutions at the two flanking positions (364 and 366) had little effect on either inactivation or K-dependence. However, unlike F364Y which had little effect on TEA block, W366Y produced a 50-fold increase in TEA block. Our results are consistent with evidence that the side chains of Trp^{365} and Trp^{366}, but not Phe^{364}, are exposed to the aqueous space and strengthen the view that residues at the amino end of the P-region are in close physical proximity to those at the carboxyl end that form part of the external mouth of the pore. Furthermore, they suggest that Trp^{365} is part of a regulatory site that controls ion-dependent gating and conduction. The effectiveness of substitutions at this position in creating non-conducting channels may be related to their ability to promote ion-dependent inactivation. We speculate that a natural Tyr variant at this position may contribute to regulation of ion-dependent gating in the distantly related HERG channel. Supported by NIH NS29473.

W-AM-H4

ANOMALOUS DEPENDENCE OF INWARD-RECTIFIER K^+ CHANNEL BLOCK ON THE SIZE OF THE BLOCKING ION.
((B. Fakler, Ch. Antz and J.P. Ruppersberg)) Dept. Physiology II, Universität Tübingen, Gmelinstr. 5, D-72076 Tübingen, Germany.
Block of inward-rectifier K^+ (Kir) channels by intracellular magnesium ions and the polyamines spermine (SPM) and spermidine is responsible for the phenomenon of voltage dependent inward rectification in Kir channels. Voltage dependence of block is usually described as the change in membrane voltage necessary for an e-fold increase in block. This parameter is assumed to correlate to the number of blocking charges times the percentage of the transmembrane electric field through which these charges are moved in the blocking reaction (electrical distance). For SPM, the most potent blocker of Kir channels, voltage dependence varies between different Kir channel subtypes, which according to the common theory may either be due to the depth by which the blocking molecules enter the channel or to the number of SPM molecules entering the channel at the same time. For Kir2.1 channels a multiple ion block is suggested by the influence of the blocker concentration on voltage dependence. This influence is not seen in Kir 1.1 channels. We show that the electrical distance of intracellular block of Kir1.1 channels by organic cations varies considerably with the volume of the blocking cation: 0.83 for tetraethylammonium, 0.93 for tetrapropylammonium and 1.44 for tetrapentylammonium (T5A) rather than with the concentration. The electrical distance is even increased up to 2.6 (for T5A) when an asparagine residue in the second transmembrane segment is mutated to aspartate (N171D). The excess electrical distance beyond unity is found to be mediated by voltagedependence of the off-rate of the blocker rather than by its on-rate as concluded from fast application experiments with T5A at inside-out patches with Kir1.1 channels. The results might be interpreted as interaction of conducting ions inside the channel with the the blocking ion mediated by the size of the blocking ion.

W-AM-H5

A 'RECTIFICATION RESIDUE' IN THE PORE (H5) REGION OF THE CARDIAC MUSCARINIC K^+ CHANNEL, GIRK1/CIR. ((C. Quinn, R. Leach, J.M. Owen, J.B.C. Findlay and M.R. Boyett)) Departments of Physiology and Biochemistry & Molecular Biology, University of Leeds, Leeds LS2 9JT, UK

During a hyperpolarizing pulse, the cardiac muscarinic K^+ channel slowly activates. The activation contributes to the inward-rectification of the channel. *Xenopus laevis* oocytes were injected with mRNA for GIRK1 and CIR (the two subunits of the muscarinic K^+ channel) and hD_2 (dopamine receptor). 36-48 hr later muscarinic K^+ current was recorded in the presence of 10 μM dopamine and 90 mM K^+ using the two-microelectrode voltage clamp technique. During a 750 ms pulse to -130 mV from a holding potential of 0 mV, current through the wild-type channel increased by 53.4 ± 4.5 % (mean ± SEM, n=6) from the start to the end of the pulse. The pore of the muscarinic K^+ channel has a ring of six negatively charged glutamate (E) residues. This was reduced to four by mutating E139 of GIRK1 to a glutamine residue. The point mutation resulted in the loss of the hyperpolarization-dependent activation: the current decreased by 17.2 ± 5.4 % (n=5) rather than increased during a pulse to -130 mV. The mutant channel also showed reduced sensitivity to Ba^{2+} (K_d at 0 mV and 90 mM K^+: wild-type channel, 80 ± 6 μM, n=5; mutant channel, 240 ± 24 μM, n=6). If the hyperpolarization-dependent activation is the result of unbinding of polyamines (Yamada and Kurachi, 1995, *J. Biol. Chem.* **270**, 9289-9294), E139 may form part of the polyamine binding site. *Supported by the British Heart Foundation and the National Heart Research Fund.*

W-AM-H6

ANOMALOUS CONDUCTION IN THE "NON-CONDUCTING" SHAKER K^+ CHANNEL MUTANT W434F
((John G. Starkus[1,2], Martin D. Rayner[2], and Stefan H. Heinemann[1]))
1: Max-Planck-Gesellschaft, AG Molekulare & zelluläre Biophysik, Jena, Germany. 2: Békésy Lab. of Neurobiology, PBRC, Univ. Hawaii, Honolulu, HI.

Gating currents were recorded from inside-out macro-patches of *Xenopus* oocytes injected with mRNA coding for the Shaker-IR mutants W434F or W434F•T449R. With external K^+ or Cs^+ solutions, the OFF currents were fast and Q_{off}/Q_{on} ratio was close to 1.0. Although these mutations were thought to abolish ion flow, significant permeation of external Na^+ ions during test pulses and marked, very slow, tail currents at negative return potentials could be observed upon complete removal of internal K^+ (panel B.). The ratios of the charge translocated during the deactivation and activation phases (Q_{off}/Q_{on}) were >> 1 in external Na^+, Li^+, and NH_4^+ solutions confirming ionic current contributions to the slow OFF currents. These slow OFF currents returned to "normal" fast kinetics and to a Q_{off}/Q_{on} ratio of about 1.0 upon addition of small amounts of internal K^+ (< 1mM), panel C. Recovery of the ON-gating charge, measured in double-pulse experiments, paralleled the time course of these tail currents. This recovery was slow in conditions of panel B and fast in A and C.

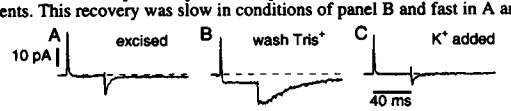

Figure: Inside-out recordings (-100, 0, -100 mV) of mutant W434F•T449R; ext. sol.: (in mM) 115 NaCl, 1.8 $CaCl_2$; int. sol.: 115 TrisCl, 1.8 EGTA. **A**: Immediately after patch excision (still some K^+ present). **B**: after wash with Tris. **C**: 1 mM K^+ added to internal solution.

W-AM-H7

A SINGLE AMINO ACID SUBSTITUTION IN THE S6 OF SHAKER DECREASES POTASSIUM AFFINITY & ALLOWS FOR SODIUM PERMEATION IN THE ABSENCE OF POTASSIUM. ((E.M. **Ogielska**, and R.W. Aldrich)) Dept. of Molecular and Cellular Physiology and Howard Hughes Medical Institute, Stanford University, Stanford CA 94305.

The delayed rectifier channel Kv2.1 readily conducts large sodium currents once potassium is removed (Ikeda & Korn, 1995). The Shaker channel however, conducts sodium quite poorly under these ionic conditions. To understand the quantitative difference in sodium permeation between these two homologous channels we focused on the sixth transmembrane domain (S6), mutating three residues in Shaker to their counterparts in Kv2.1. In the absence of potassium, the S460G:A463C:T469V triple mutant confers a substantial sodium permeability onto the Shaker channel. We were able to further localize the effect to the residue at position 463. An alanine to cysteine mutation at 463 in S6 is sufficient to alter the sodium permeability of the channel when potassium is removed. The observed sodium currents in both the triple mutant and A463C can be blocked by external TEA and Agitoxin, a specific Shaker channel blocker, indicating that the currents are indeed due to sodium permeating the Shaker channel. Neither S460G nor T469V can reproduce the changes in selectivity observed with S460G:A463C:T469V. Under physiological conditions both the wildtype channel and all the mutants are highly potassium selective. The sodium currents in the A463C mutant can also be blocked with mM potassium indicating that potassium binds to the pore with a higher affinity than sodium. Although the wildtype Shaker channel conducts some sodium in the absence of potassium it does so only if extreme care is taken to eliminate potassium. The wildtype channel must have a very high affinity potassium binding site, the affinity of which is influenced strongly by the nature of the amino acid residue at position 463.

W-AM-H8

DIFFERING SELECTIVITIES OF SUB-CONDUCTANCE STATES IN A MUTANT *SHAKER* CHANNEL ((J. **Zheng** and F. J. Sigworth)) Dept. of Cellular and Molecular Physiology, Yale Univ. School of Medicine, New Haven, CT 06520

We have been studying a *Shaker*-NGK2 channel chimera containing the mutation T442S, which is very close to the presumed selectivity filter. It shows sub-conductance states as the channel activates and deactivates (Zheng and Sigworth, Biophys. J. (Abstract) 70:A190, 1996). The sublevel phenomenon persists when K^+, Rb^+, and NH_4^+ are used as the permeant ions. We find that the main open level and sublevels have different selectivites. At all the voltages tested the main open state is more permeable to Rb^+ while the sublevel states are more permeable to K^+; NH_4^+ is intermediate.

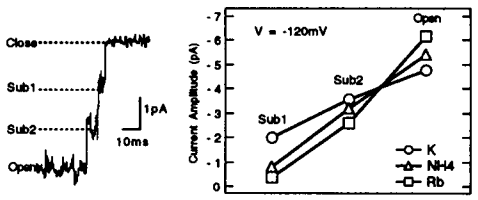

The current trace shows channel deactivation at -120mV with external K^+. The graph shows current amplitude at -120mV with the given external ions.

W-AM-H9

BA^{2+} ACTIVATION OF MSLO CA^{2+}-ACTIVATED K CHANNELS ((**F.T. Horrigan** & R.W.Aldrich)) Stanford University School of Med., Dept. of Molecular and Cellular Physiology, HHMI, Stanford, CA 94305

Ba^{2+} has long been recognized to block Ca^{2+}-activated K channels in a voltage-dependent manner by occupying the channel pore. Here we show that Ba^{2+} also can activate Ca^{2+}-activated K channels, presumably by interacting with Ca^{2+}-binding sites. mSlo Ca^{2+}-activated K channels were expressed in *Xenopus* oocytes and macroscopic K currents were recorded from inside-out patches. Solutions containing various concentrations of Ba^{2+}, 2 mM EGTA, and no added Ca^{2+} were applied to the cytoplasmic side of the membrane ($[Ca^{2+}] < 10$ nM). In the absence of Ba^{2+} and Ca^{2+}, I_K begins to activate around +70 mV. Application of 10 μM Ba^{2+} shifts the threshold for activation by -40 to -50 mV such that I_K evoked at +80 mV is greatly enhanced by Ba^{2+}. In addition, Ba^{2+} speeds I_K activation and slows deactivation. These effects of 10 μM Ba^{2+} are similar to the actions of 1 μM Ca^{2+}. However activation of mSlo by Ba^{2+} is only evident at voltages <+100 mV because Ba^{2+} block at more depolarized voltages reduces I_K. Ba^{2+}-activation was more obvious with the mSlo mutant R207Q. The mutant channel activates at more hyperpolarized voltages than mSlo; thus Ba^{2+} activation can be observed at voltages where Ba^{2+}-block is minimal. Ba^{2+} activation was also observed in recordings of single native Ca^{2+}-activated K channels from PC12 cells. The effect of Ba^{2+} on channel activation may provide important information concerning the selectivity of the channel's Ca^{2+}- binding sites.

CARDIAC E-C COUPLING

W-AM-I1

MUSCARINIC AGONIST INCREASES NA/CA EXCHANGE CURRENT, CA2+ TRANSIENTS AND CONTRACTIONS IN VENTRICULAR MYOCYTES. ((Lev Protas, Jian-Bing Shen, Tomoaki Saeki and **Achilles Pappano**)) Department of Pharmacology, University of Connecticut Health Center, Farmington, CT 06030 (Spon. Ramadan Sha'afi)

Carbachol (CCh, 3-300 μM) increased the early component of isotonic contractions in single guinea pig ventricular myocytes superfused with Tyrode's solution (36°C, 5.4 mM $[Ca^{2+}]_o$) and stimulated externally at 0.2 Hz. Carbachol (EC_{50}≈18 μM) acted at muscarinic receptors (mAChR) of the the M_2 subtype because the CCh effect was more sensitive to block by AF-DX 116 (M_2-selective) than pirenzepine (M_1-selective). Voltage clamp steps to -30 mV evoked I_{Na} followed by a tail current carried by Na/Ca exchange ($I_{Na/Ca}$); CCh increased $I_{Na/Ca}$ reversibly via mAChR occupancy. CCh did not change the L-type Ca^{2+} current (I_{Ca}) but reversibly increased intracellular Ca^{2+} transients by an effect via sarcoplasmic reticulum (SR). $I_{Na/Ca}$ and the early contraction component were blocked in ryanodine (1-10 μM); CCh did not restore either in the presence of ryanodine. After conditioning pulses to load the SR, 10 mM caffeine evoked an inward current at -70 mV due to $I_{Na/Ca}$. CCh increased the caffeine-induced charge movement indicating that muscarinic agonist further augmented SR Ca^{2+} stores. We propose that CCh-induced stimulation of Ca^{2+} transients and contractions arises from an increased Na^+ entry by occupancy of M_2 receptors that alters Na/Ca exchange and eventually augments SR Ca stores. This hypothesis accounts for the ability of CCh to enhance excitation-contraction coupling without significantly changing I_{Ca} in guinea pig ventricular myocytes.

W-AM-I2

CA^{2+} RELEASE FROM THE SARCOPLASMIC RETICULUM TRIGGERED BY REVERSE MODE NA/CA EXCHANGE IS SLOW ((**Karin R. Sipido**, Micheline Maes*, Frans Van de Werf)) Lab. of Exp. Cardiology, University of Leuven, B-3000 Belgium; *Lab. of Electrobiology, University of Antwerp, Belgium.

Ca^{2+} entry through the L-type Ca^{2+} channel is a very efficient trigger for Ca^{2+} release from the sarcoplasmic reticulum (SR). It has been proposed that Ca^{2+}entry through the Na/Ca exchanger (NCX) also participates in triggering release. We have examined the characteristics of this latter trigger mechanism in comparison to L-type Ca^{2+} current (I_{CaL}). Guinea-pig ventricular myocytes were studied in whole-cell voltage clamp mode; the pipette solution contained: (in mM) K-aspartate 120, KCl 20, NaCl 20, $MgCl_2$ 0.5, MgATP 5, fluo-3 0.06 (or fura-red 0.07 and fluo-3 0.03), HEPES 10, pH 7.20. The external solution contained: (in mM) NaCl 137, KCl 5.4, $MgCl_2$ 0.5, $CaCl_2$ 1.8, dextrose 10, HEPES 11, pH 7.40 (T = 35°C). Steady state loading of the SR was obtained by conditioning steps to +60 mV and was unaffected by block of I_{CaL} (nisoldipine 20 μM). Ca^{2+} release was examined during test depolarizations to -20 mV up to +70 mV. In control conditions, the maximal rate of rise of $[Ca^{2+}]_i$ occurred at +10 mV, and the relation between dCa/dt and membrane potential was bell-shaped. After block of I_{CaL}, rapidly rising $[Ca^{2+}]_i$ transients which were blocked by ryanodine (10 μM), could still be observed. dCa/dt was linearly related to the membrane potential but was less than in the presence of I_{CaL} (at +70 mV, 0.7±0.1 of the peak rate of rise at +10 mV with I_{CaL}, mean±SEM, n=6). After block of I_{CaL}, Ca^{2+} release occurred with a delay: time to peak dCa/dt was 39±4 ms at +70 mV up to 90±16 ms at +10 mV, versus 8±0.3 ms at +10 mV with I_{CaL} (n=6). The onset of Ca^{2+} release coincided with a clear inward shift of the Ni^{2+}-sensitive NCX current. Maximal Ca^{2+} entry through NCX was 2.6±0.5 pA/pF at +70 mV, comparable to Ca^{2+} entry through I_{CaL} at +40 mV (2.5±0.5 pA/pF). However, no delay was observed with I_{CaL} at +40 mV (time to peak dCa/dt 9±0.8 ms). We conclude that Ca^{2+} entry through the NCX is less efficient than I_{CaL} in triggering SR Ca^{2+} release.

W-AM-I3

DEPENDENCE OF REVERSE Na/Ca EXCHANGE ON INFLUX OF Na VIA Na EFFECT OF Na CURRENT ON Na-Ca EXCHANGE CURRENT: EVIDENCE FOR A FUZZY SPACE. ((Jun Li and John H.B.Bridge)) CVRTI, Univ. Utah, Salt Lake City, UT 84112

We use a whole cell voltage clamp technique, in combination with rapid perfusion to isolate reverse Na/Ca exchange current (I_{ex}) and controlled Na currents. Because Na currents enhance triggering of SR Ca release by reverse Na-Ca exchange we tested the hypothesis that Na influx through sarcolemmal Na channels enhances reverse Na/Ca exchange current. We first activated (by voltage-clamping from -80 to -40 mV) a series of controlled Na currents (I_{Na}) (pipette contained a cesium based solution with 10 mM Na , 14 mM BAPTA) while perfusing the cells with 20 mM Na, 100 nM Ca, and 1 mM EGTA. We activated outward I_{ex} by rapidly switching to a zero Na, 2.7 mM Ca solution. The magnitude of Ni sensitive I_{ex} depended on the number, frequency, and size of the preceding I_{Na}, with I_{ex} being larger after application of increasing numbers (n=4), frequency (n=3), and size (n=42) of I_{Na}; Ouabain (0.5 mM) led to a larger peak I_{ex} (up to more than 2-fold, n=3); Dialyzing cells with XIP resulted in attenuation of the increases of I_{ex} in cells that received I_{Na} trains (n=3). With 40μM TTX-containing solution, I_{Na} was blocked and so was the corresponding increase in I_{ex} (n=6). Increasing the interval between the end of an I_{Na} train and activation of I_{ex} made I_{ex} become progressively smaller with an approximate $t_{1/2}$ of 150 ms (n=3). We conclude that under these experimental conditions the activity of reverse exchange is dependent on cellular Na accumulation produced by I_{Na} possibly in a subsarcolemmal or fuzzy space. This is consistent with the idea that I_{Na} enhances triggering by reverse exchange.

W-AM-I4

EFFECTS OF Ca^{2+} CHANNEL BLOCK AND TEMPERATURE ON E-C COUPLING IN CAT VENTRICULAR MYOCYTES. ((J. Andrew Wasserstrom)) Department of Medicine, Northwestern Medical School, Chicago, IL 60611.

Recent studies indicate that Na-Ca exchange contributes to triggering of cardiac contraction independently from L-type Ca^{2+} current (I_{Ca}). The purpose of this study was to determine the conditions that favor activation by the two mechanisms and to quantify their respective contributions. Cell shortening was measured during patch clamp experiments performed using the discontinuous voltage clamp (20KHz) in isolated cat ventricular myocytes with solutions containing normal Na^+ and K^+ concentrations (no Cs^+, 35°C). In control, the voltage dependence of contraction (holding potential =-40mV) was sigmoidal, with activation occurring at a test potential of -20mV and reaching a peak near +20mV above which contraction remained fairly constant up to +90mV. Addition of either Cd^{2+} (20μM) or nifedipine (10μM) caused voltage dependent block of contraction that closely mimicked that of I_{Ca}. Its voltage dependence was bell-shaped such that there was little effect of either agent below -10mV or above +50mV but extensive block between those voltages, with maximal block (50-60%) occurring at about +20mV. All remaining contraction was blocked by Ni^{2+} (4-5mM) or ryanodine (10μM), suggesting that the Cd^{2+}/nifedipine-insensitive contraction resulted from activation of reverse Na-Ca exchange and SR Ca^{2+} release. The voltage dependence of contraction was sigmoidal at experimental temperatures of 34°C and above but was bell-shaped at 30°C and below. Superfusion with Cd^{2+} reduced contraction at +10mV to 6±3% of control at 25°C but had much less effect at 34°C (65±13% of control, p<0.01 compared to 25°C). These results suggest that 1) the contributions of I_{Ca} and the exchanger to triggering are voltage dependent, with a bell-shaped contribution of I_{Ca} that is superimposed upon a fairly linear component derived from the exchanger; 2) the contribution of the exchanger is temperature-sensitive and is only apparent at physiological temperatures; and 3) since the normal action potential overshoot is about +20-+40mV, the contributions of the two mechanisms are nearly equal at physiological voltages and temperatures.

W-AM-I5

MITOCHONDRIAL CALCIUM UPTAKE IN PATCH CLAMPED VENTRICULAR MYOCYTES. ((Z. Zhou and D.M. Bers)) Department of Physiology, Loyola University Chicago, Maywood, IL.

We measured mitochondrial (Mito) free [Ca] ($[Ca]_M$) in ferret and cat ventricular myocytes which were loaded with indo-1/AM under conditions that produced strong Mito loading and with cytosolic [Ca] ($[Ca]_C$) measured by contraction (see Zhou & Bers, this volume). Ca transients were activated by Ca entry via Na/Ca exchange to avoid I_{Ca} rundown effects during dialysis. While cytosolic indo was being dialyzed out Ca transients were due to both Mito and cytosolic indo. Basal Ca transients showed the same kinetics as cell contraction (and $[Ca]_C$). When stronger & longer pulses (e.g. 4 sec +110 mV) were repetitively applied to elevate both resting and peak $[Ca]_C$ the indo showed a slower component reflecting a change in $[Ca]_M$ (completely blocked by inclusion of the Mito Ca uniport blocker RU360 in the pipet). Mn quench of cytosolic indo gave similar results, but with *pure* $[Ca]_M$, uncontaminated by $[Ca]_C$. With basal stimulation there was no $[Ca]_M$ transient. With progressively strong loading pulses (i.e. resting $[Ca]_C$ >300 nM) clear Mito $[Ca]_M$ transients emerged associated with large contractions (L) and $[Ca]_C$ transients (Fig). The $[Ca]_M$ signal was delayed by ~1 sec with respect to the $[Ca]_C$ transient and declined slowly. We conclude that $[Ca]_M$ transients are minimal until diastolic $[Ca]_C$ is elevated and then they are much slower than $[Ca]_C$ transients.

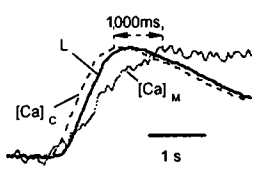

W-AM-I6

CALCIUM TRANSPORT IN PHOSPHOLAMBAN KNOCKOUT MOUSE: RELAXATION AND ENDOGENOUS CaMKII EFFECTS

((L. Li*, E.G. Kraniast and D.M. Bers*)), *Dept. Physiology, Loyola University Chicago, Maywood, IL 60153. †Dept. Pharmacology and Cell Biophysics, Univ. Cincinnati, College of Medicine, Cicinnati, OH 45267

We studied Ca transients and contractions in ventricular myocytes isolated from wild type (WT) mice and those in which the phospholamban (PLB) gene was knocked out (PLB-KO, Luo *et al.*, *Circ Res*,75:401, 1994). We find that the time constant (τ) of $[Ca]_i$ decline during steady state twitch (SSTw) is much faster in PLB-KO than WT myocytes (112±6 ms *vs* 188±14 ms, p<0.0001). There was no significant increase in the amplitude of SSTw Ca, transients or contractions, but the SR Ca load was higher in PLB-KO mice, based on $\Delta[Ca]_i$ during rapid caffeine-induced contractures (CafC; 395±34 nM in WT, 578±45 nM in PLB-KO, p<0.01). The τ for $[Ca]_i$ decline of the CafC (2.2±0.2 sec in WT *vs.* 3.2±0.2 sec in KO, p<0.01) suggests slower Na/Ca exchange in the PLB-KO. Integrated Ca flux analysis in WT shows that 91% of Ca during relaxation of the SSTw is removed by the SR Ca-ATPase, 8.6% by Na/Ca exchange and 0.5% by slow mechanisms. In PLB-KO, these values are 97%, 3.2% and 0.1%, respectively, consistent with stronger SR Ca-pump activity. Both WT and PLB-KO myocytes show rest potentiation of contraction and slower $[Ca]_i$ decline at the post-rest twitch (PRTw). This indicates that acceleration of the SSTw $[Ca]_i$ decline and relaxation cannot be attributed solely to PLB. The CaMKII inhibitor KN-93 (1 μM) abolished the acceleration of SSTw τ (*vs* PRTw) in PLB-KO (120±5 ms in SS and 115±6 ms in PR). We conclude that the PLB-KO (*vs* WT) myocytes have higher SR Ca-ATPase activity, higher SR Ca load & reduced Na/Ca exchange and they also retain a CaMKII-dependent acceleration of SSTw $[Ca]_i$ decline.

W-AM-I7

DIASTOLIC Ca EFFLUX FROM SR IN CAT ATRIAL PACEMAKER CELLS AND Ca-OVERLOADED MYOCYTES. ((R.A. Bassani,., J.W.M. Bassani, S.L. Lipsius, & D.M. Bers)) CEB/FEEC, Universidade Estadual de Campinas, Brazil and Department of Physiology, Loyola University Chicago, Maywood, IL USA

SR Ca release may play a role in diastolic depolarization of cat right atrial latent pacemaker cells (AtLP; Zhou & Lipsius, *J. Physiol., 466*:263, 1993). This seems at odds with the very slow rate of diastolic SR Ca efflux in ventricular myocytes (Bassani & Bers, *Biophys. J., 68*:2015, 1995). Indeed, resting $[Ca]_i$ does not rise in ventricular myocytes even during inhibition of both the SR Ca pump and Na/Ca exchange. Here we compared diastolic $[Ca]_i$ changes induced by block of the SR Ca-pump and Na/Ca exchange (by thapsigargin, TG. and Na-free solution) in cat sino-atrial node cells (SAN), AtLP, and atrial myocytes (AtMy) at 23°C. AtLP developed a slow Ca transient (Fig) resulting in SR Ca depletion (in <5 min of TG exposure). In SAN, this $[Ca]_i$ transient was absent and caffeine still induced $[Ca]_i$ increase 5 min after TG addition. AtMy stimulated at 0.5 Hz behaved like SAN, but Ca-overloaded AtMY behaved more like AtLP (slow resting Ca transient in TG). SR Ca depletion by TG did not alter spontaneous activity in SAN, but reduced or abolished it in AtLP. We conclude that diastolic SR Ca efflux is involved in the generation of spontaneous activity in both AtLP and Ca-overloaded AtMy, but not SAN. *Support: FAPESP (96/1600-4) and NIH (HL-27652 & 30077)*

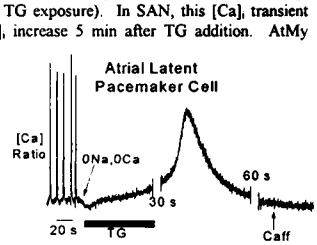

W-AM-I8

EXCITATION-CONTRACTION COUPLING IN TRANSGENIC MYOCYTES OVEREXPRESSING CARDIAC CALSEQUESTRIN. ((Y.J. Suzuki, Y. Kobayashi, M. Morad and L.R. Jones*)) Dept. of Pharmacology, Georgetown Univ., Washington, DC 20007 and *Krannert Inst. of Cardiology, Indiana Univ., Indianapolis, IN 46202. (Spon. by J.J. Feher)

Calsequestrin (CSQ) is a Ca^{2+}-binding protein localized in the sarcoplasmic reticulum (SR). The present study examined ventricular myocytes from transgenic mice overexpressing CSQ using the cardiac α-MHC promoter. Hearts from CSQ mice were hypertrophied (1.6-fold in mass compared to their non-transgenic littermates) showing often areas of fibrosis. Western blot analysis showed that CSQ mice had 18-fold increase in ventricular CSQ content. Freshly isolated ventricular myocytes had distinctive appearance showing no clear striation and significant increase in cell capacitance (240.6±12.8, n=52 vs 153.5±7.0, n=19). Whole-cell clamped myocytes from CSQ mice dialyzed with 0.1 or 2 mM fura-2 showed very large Ca^{2+}- release from the SR in response to caffeine-exposure, suggesting that SR was over-loaded with Ca^{2+}. In CSQ-overexpressing myocytes dialyzed with 0.1mM fura-2, caffeine-induced $\Delta[Ca^{2+}]_i$ ranged from 1 to 3 μM (compared to 600nM in control), and Na^+-Ca^{2+} exchange current ($I_{Na/Ca}$) was 6.7±0.6 pA/pF (compared to 1.7 pA/pF). Surprisingly, significant level of $I_{Na/Ca}$ was measured even in myocytes dialyzed with 2mM fura-2, but not in control myocytes. Depolarization to potentials positive to +60mV failed to trigger Ca^{2+} release, suggesting that large increase in caffeine-induced $I_{Na/Ca}$ results from increased release of Ca^{2+} from the SR rather than compensatory overexpression of the exchanger. In contrast to caffeine-induced Ca^{2+} release, I_{Ca}-induced Ca^{2+} release was significantly smaller and inactivation of I_{Ca} was slower in CSQ vs control myocytes. These results show that overexpression of CSQ in cardiac myocytes increases Ca^{2+} content of SR, but decreases the efficacy of I_{Ca}-induced Ca^{2+} release. It is intriguing to speculate that overexpression of CSQ may be in part responsible for cardiac hypertrophy and failure. (Supported by NIH HL16152)

W-AM-I9

EFFECTS OF FK506 ON THE $[Ca^{2+}]_i$ TRANSIENT IN RAT VENTRICULAR MYOCYTES. ((W.H. duBell[1], P. Wright[2], W.J. Lederer[3] and T.B. Rogers[1])) Dept. of Biochem. & Molecular Biology[1], Dept. of Surgery[2] and Dept. of Physiology and The Medical Biotechnology Center[3], University of Maryland School of Medicine[1,2] and the University of Maryland Medical System[2], Baltimore MD 21201.

The immunosuppressant drug FK506 modifies ryanodine receptor (RyR) Ca^{2+} flux in lipid bilayers through the associated protein FKBP12. Further, it increases the $[Ca^{2+}]_i$ transient and alters Ca^{2+} spark kinetics in isolated cardiac cells (Xiao et al., Biophys J. 70:A245, 1996). Ca^{2+}-sensitive fluorescent dyes were used to further examine the role of the sarcoplasmic reticulum (SR) in the effects of FK506 on $[Ca^{2+}]_i$ transients in rat ventricular myocytes (30 °C,1.0 mM $[Ca^{2+}]_o$). Similar to previous studies, we found a reversible increase of 22% in the magnitude of field-stimulated (2 Hz) fluo-3-measured $[Ca^{2+}]_i$ transients following exposure to 25 μM FK506. However, when voltage clamp depolarizations, in the presence of K^+ channel blockers (Ca^+, 4AP and TEACl), were used to activate $[Ca^{2+}]_i$ transients in cells loaded with indo-1 free acid through the voltage clamp pipette, neither the $[Ca^{2+}]_i$ transient nor I_{Ca} was increased by FK506. Nor was there an increase in the $[Ca^{2+}]_i$ transient during voltage clamp drives from -70 to 0 mV (100 ms pulses) in the absence of Na^+ and K^+ channel blockers. However, there was an inward shift in the current recorded during each pulse. Finally, FK506 prolonged the action potential (AP) in cells loaded with indo-1 AM, increasing the time to 90% repolarization by 144% (n=2). The AP prolongation was accompanied by an increase in the $[Ca^{2+}]_i$ transient. These results suggest that, in addition to any actions on the RyR, FK506 decreases an outward current in rat ventricular myocytes. (Supported by NIH HL-27867)

MOLECULAR MOTORS

W-AM-J1

CORRELATED MOTION OF ACTIN FILAMENT SEGMENTS ON EITHER SIDE OF A SINGLE ATTACHED CROSSBRIDGE. ((A. D. Mehta and J. A. Spudich)) Dept of Biochemistry, Stanford University, Stanford, CA 94305.

A number of experiments have addressed motion generated by actin and myosin, both in well ordered arrays within muscle myofibrils and at the single molecule level. However, past experiments have not measured independently movement at different points within a single actin filament. Using a sensitive laser trap assay for single myosin molecule activity, we have observed tightly correlated motion of actin filament segments on either side of a given myosin crossbridge. These experiments allow us to more precisely define the class of models which can be invoked to explain actomyosin driven motility.

W-AM-J2

QUANTAL NATURE OF SHORTENING IN SINGLE SARCOMERES OF SINGLE MYOFIBRILS. ((Paul Yang, Tsukasa Tameyasu, **Gerald H. Pollack**)) Center for Bioeng. 357962, Univ. of Wash, Seattle WA 98195

Single myofibrils of honeybee flight muscle were examined in relaxing solution. The prestretched myofibril was released slowly over a period of several seconds. To measure single sarcomere dynamics, the striation pattern was projected onto a 512-element photodiode array, scanned every 50 ms. The length of a selected sarcomere was reckoned as the spacing between contiguous A-band centroids. The resulting sarcomere-shortening records were generally stepwise. To measure step size, we developed an algorithm that selects the best linear fit to each pause and computes the size of the step included between two consecutive pauses. The histogram of step size shows distinct peaks spaced every 2 - 3 nm (far smaller than the photodiode-element spacing). This implies that the size of the sarcomere shortening step may be a multiple of a 2 - 3 nm quantum. For the ~650 steps analyzed so far, the best fit for inter-peak spacing is 2.48 nm, or 1.24 nm per half-sarcomere. Thus, the size of the shortening step per half-sarcomere may well be an integer multiple of 1.24 nm. This striking result remains tentative because some histogram peaks are less prominent than others. We are taking measures to ameliorate this by reducing noise in the sarcomere-length detection system and by including additional data points in the histogram.

W-AM-J3

NON-PROCESSIVE MICROTUBULE MOTILITY BY A MONOMERIC KINESIN. ((**E. C. Young** and J. Gelles)) Biochemistry Department, Brandeis University, Waltham MA 02254-9110.

A single molecule of kinesin can move continuously along the microtubule lattice for many enzymatic turnovers. We studied two biotinated N-terminal fragments of *Drosophila* kinesin heavy chain which drive unidirectional microtubule motion when attached at high surface density to streptavidin-coated coverslips. K448-BIO is a dimer with two active sites and maximum velocity 800 nm/s (like intact kinesin), and K340-BIO is a monomer with one active site and maximum velocity 90 nm/s. From microtubule trajectories recorded by video microscopy, the component of instantaneous velocity parallel to the microtubule axis was calculated. Methyl cellulose was added to prevent diffusion of the microtubule away from the surface, and had no effect on velocity at high surface densities of either enzyme. Mean velocity decreased for both enzymes as surface density was reduced. At low surface densities, the distribution of instantaneous velocities produced by K448-BIO is bimodal with peaks near 0 and 800 nm/s, but the K340-BIO velocity distribution is unimodal with its peak below 90 nm/s. Temporal autocorrelation analysis of velocities shows that K448-BIO motility contains episodes of sustained unidirectional movement whose durations scale with microtubule length, interrupted by episodes of random motion. This is consistent with random diffusive encounters of the microtubule with single K448-BIO dimers that produce processive motion at high speed. K340-BIO velocity correlation times are much shorter. This implies that more than one K340-BIO molecule are required to drive continuous unidirectional microtubule motion, and that during a significant fraction of the enzymatic turnover cycle the K340-BIO active site cannot attach to a microtubule.

W-AM-J4

A MOLECULAR ROSETTA STONE: DOES THE CRYSTAL STRUCTURE OF THE KINESIN MOTOR DOMAIN REVEAL AN EVOLUTIONARY LINK BETWEEN MOLECULAR MOTORS AND GTP-HYDROLYZING ENZYMES?

((**F. Jon Kull**, Elena Sablin, Ron Vale, and Robert Fletterick)) Department of Biochemisty and Biophysics, UCSF, San Francisco, CA, 94143

Kinesin is the founding member of a large superfamily of microtubule-based motor proteins that perform force-generating tasks such as organelle transport and chromosome segregation. Recently, we have determined the crystal structures of both the human kinesin motor domain (a plus-end directed motor) and the motor domain of NCD (a minus-end directed motor). Both domains, which share a 40% amino acid identity, are remarkably similar, consisting primarily of a single α/β arrowhead-shaped domain with dimensions of 70 x 45 x 45 Å. Remarkably, this region exhibits a striking similarity to the core of the catalytic domain of the actin-based motor myosin. Although kinesin and myosin have virtually no amino acid sequence identity and exhibit distinct enzymatic and motile properties, our results suggest these two classes of mechanochemical enzymes evolved from a common ancestor and share a similar initial strategy for force-generation which is then specialized for directionality (kinesin vs. NCD), polymer substrate (actin-myosin vs. kinesin-microtubules), and enzymatic activity. Furthermore, comparison of kinesin with several G-proteins ($p21^{ras}$, EF-Tu, and transducin-α) shows intriguing structural and functional similarities, indicating these NTPases share a common mechanism for sensing nucleotide state and converting this signal into the initial conformational changes necessary for many diverse cellular functions. An evolutionary pathway describing a relationship between these highly divergent proteins is also presented.

W-AM-J5

FORCE GENERATION IN THE COCHLEAR OUTER HAIR CELL UNDER VOLTAGE CLAMP.

((**K. H. Iwasa** and M. Adachi)) Biophysics Section, LCB, NIDCD, NIH, Bethesda, MD 20892-0922

Among biological motilities, most of which depend on chemical energy, the outer hair cell (ohc) from the mammalian cochlea is unique in that it directly uses electrical energy. To determine the dependence of the force production of the ohc on the membrane potential, we performed a series of experiments in which an elastic probe was attached to the cell near the cuticular plate and the cell was driven with voltage pulses delivered from a patch pipette under whole-cell voltage clamp. The axial elastic modulus was also determined in the same experimental configuration by moving the patch pipette. We found that the isometric force generated by the ohc has a maximum slope of around 0.1 nN/mV, somewhat smaller than 0.15 nN/mV, predicted by an area motor model (J. Acoust. Soc. Am. 1994, 96:2216) based on a mechanical istotropy but larger than earlier reports in which the membrane potential was not controlled. The area motor model assumes two states for the membrane motor and further assumes that displacement of the cell is a sum of motor displacement and elastic displacement of the membrane. Transitions between the two states of membrane motor accompany charge transfers across the membrane and mechanical displacements, both of which have been determined earlier by capacitance experiments. The axial elastic modulus obtained, however, was on the average 530 nN, about a half of the value expected from the mechanical isotropy of the membrane. To account for this difference, we extended the area motor theory to the condition of mechanical orthotropy, and found that the value for the isometric force generated by the cell is approximately proportional to the axial stiffness. This theory predicts 80 % of the force obtained in the present experiment.

W-AM-J6

MICROTUBLE ORGANIZING CENTER AND ASSOCIATED VESICLE MOVEMENTS OF LIVING T LYMPHOCYTES VISUALIZED BY MODULATED POLARIZATION MICROSCOPY.

((**Jeffrey R. Kuhn** and Martin Poenie)) Dept. of Zoology, University of Texas, Austin, TX 78712, USA

Many types of cells exhibit cytoplasmic polarity during some part of their life history. Examples of this polarity are seen in bud site selection of yeast, animal-vegetal axis of oocytes and the polarized organization of the cytoskeleton in migrating cells and during T cell mediated killing of target cells. In T cell, killing via the secretory pathway involves movements of the cytoskeleton and coordinated directional movement of vesicles. To study these cytoskeletal and vesicles movements, we have developed a new type of microscopy called modulated polarization microscopy. Here we selectively image weakly birefringent structures such as vesicles and cytoskeletal elements using the principle that birefringence depends on the polarization angle of the illuminating light. Here, we modulate polarization angle illuminating light at a fixed rate while viewing the specimen between crossed polarizers. This causes birefringent structures to oscillate in intensity. Video images are then processed using a single frequency Fourier filter which passes only those elements in the image that oscillate at the right frequency. Using this approach we have been able to image the microtubule organizing center, microtubules, and their associated vesicles in living T lymphocytes and their cognate target cells.

W-AM-J7

THE ROLE OF TAU IN NEURITE OUTGROWTH AND GROWTH CONE MOTILITY

((**Canwen Liu***, Gloria Lee# and Daniel Jay*)) *Department of Molecular and Cellular Biology, Harvard University, Cambridge, MA 02138 and #Center for Neurologic Diseases, Harvard Medical School, Boston, MA 02115.

The microtubule-associated protein tau is located in the axon and central domain of the growth cone. It promotes tubulin polymerization and binds and stabilizes microtubules *in vitro*. Antisense inhibition of tau expression in cerebellar neurons inhibited axogenesis (Caceres and Kosik, 1990), whereas genetic knockout of tau had little effect on neurite structure (Harada *et al.*, 1994). As such, the *in vivo* function of tau remains unclear. Here we have used microscale chromophore assisted laser inactivation (micro-CALI) to study the role of tau in chick DRG neurite outgrowth and growth cone motility. Micro-CALI targets laser energy to specifically inactivate proteins by binding them with non-blocking antibodies conjugated with chromophore, malachite green. Inactivation of tau within single growth cones caused a significant decrease in neurite extension rate (≈ 2 fold) and lamellipodial retraction but filopodial motility was not affected. No effect on growth cone behavior was observed when anti-tau was replaced by nonimmune IgG and micro-CALI of other proteins showed markedly different effects on growth cone behavior. Our findings support a critical function for tau in neurite extension and also suggest a novel role in lamellipodial motility at the growth cone leading edge.

W-AM-J8

THE 74-kD INTERMEDIATE CHAIN, A REGULATORY COMPONENT OF CYTOPLASMIC DYNEIN?

((**W. Steffen**[1], J. L. Hodgkinson[2], D. G. Weiss [3], and S. A. Kuznetsov[3]))[1] Univ. Vienna, Inst. Biochem. & Molec. Cell Biol., Biocenter, Dr. Bohrgasse 9, A-1030 Vienna, Austria. [2] Imperial College of Sch. Med.,Natl. Heart & Lung Inst., Dovehouse Street, London SW3 6LY, UK., [3] Univ. Rostock, Inst. Zoology, Universitatsplatz 2, 18055 Rostock, Germany. (Spon. J.L.Hodgkinson).

Cytoplasmic dynein is one of the major motor proteins involved in intracellular transport. It is a protein complex consisting of two heavy chains, three intermediate chains and several light chains. Two monoclonal antibodies (m74-1 and m74-2) specific for the intermediate chain labelled the base of the motor complex by immuno-EM of negatively stained cytoplasmic dynein from bovine brain. The localization of the intermediate chain at the base of cytoplasmic dynein indicated that the intermediate chain might be involved in docking the motor complex onto its target. Both monoclonal antibodies (m74-1 and m74-2) also recognized the intermediate chain in cytoplasmic extracts of Xenopus oocytes by SDS-PAGE immunoblot. Allan has demonstrated that cytoplasmic dynein is essential for membrane transport and tubular network formation along microtubules in vitro (J. Cell Biol. 128, 879-891 1995). However, when cytoplasmic extracts of Xenopus oocytes were incubated with any of our monoclonal antibodies (m74-1, m74-2), no organelle movement and network formation was observed. The membrane transport was already blocked at an antibody concentration of about 10 µg/ml. In contrast to these observations, no effect on organelle movement and tubular network formation was observed in the presence of a control antibody at concentrations as high as 0.5 mg/ml. Our data presented here indicate that the intermediate chain could be involved not only in docking the complex to organelles but in regulating motor activity as well.

W-AM-J9

UNCAGING PEPTIDE BLOCKERS OF CaCM AND MLCK STOPS EOSINOPHIL MOTILITY.

((**F. S. Fay**, S. H. Gilbert, R. M. Drummond, M. Ikebe and J. W. Walker*)) Dept. of Physiology, UMMC, Worcester MA and *Dept. of Physiology, Univ. of Wisconsin, Madison, WI.

Roles have been suggested for myosins I and II in nonmuscle cell motility, mostly from genetic knock-out experiments and immunocytochemistry. To investigate myosins' roles acutely, on a time-scale of changes in $[Ca^{2+}]_i$ and cell direction, we developed photolabile analogs of two peptides that on photolysis inhibit specifically CaCM binding to myosin light-chain kinase (MLCK) and MLCK phosphorylation of myosin light chains. Both peptides should block activation of myosin II by phosphorylation of its light chains. The MLCK inhibitor (LSM1) should block only that reaction, whereas the CaCM blocker, RS20, could also interfere with other calmodulin-dependent processes, including myosin I activity. We injected either peptide along with a fluorescein-dextran marker into newt eosinophils and recorded their motion for 5-min periods before and after exposure to UV to photorelease active peptide. Both peptides blocked motility for several minutes, including locomotion across the subtratum, expansion of lamellipods, organized granule flow and detachment of the rear of the cell from the substratum. Identical UV exposures of uninjected cells and cells injected with a doubly-caged peptide, from which photolysis released an inactive peptide and two molar equivalents of the caging group, caused no discernible changes in motility. Cells arrested by phororelease of either peptide formed lamellae at several sites, which after several minutes surrounded most of the granular region and ruffled at their outer edges. We conclude that myosin II is principally responsible for locomotion, granule flow and major shape changes in these cells, but not formation or ruffling of lamellae.

W-AM-K1

PROTEINS AS LOW-REORGANIZATION-ENERGY MEDIA FOR CHARGE-TRANSFER REACTIONS ((L. I. Krishtalik, E. L. Mertz and V. V. Topolev)) A. N. Frumkin Inst. of Electrochemistry, Russian Academy of Sciences, Leninskii prosp. 31, 117071 Moscow, Russia. (Spon. by W. A. Cramer)

A relatively rigid fixation of highly polar, mainly peptide groups in the protein's structure has two interconnected consequences. First, these dipoles create some permanent electric field. Second, the low mobility of the dipoles results in restrictions of their reorientation in an electric field, i.e., in the low dielectric constant of the protein. This decreases markedly the reorganization energy for any intraprotein charge transfer, which is one of the physical reasons for the catalytic effect of enzymes. For globular enzymes, an analysis in the framework of a continuum dielectric model reveals the tendencies to optimum disposition of reactants and an optimum globule size that agree with experimental data. For an independent proof of the low reorganization energy of a protein, we measured the Stokes shift for a dye proflavine in a complex with α-chymotrypsin. Comparison of these data with analogous data for a free dye in different solvents confirms the low reorganization characteristics of the protein. (Supported by grants from the ISF (MD9300), INTAS (93-2852) and RFBR (96-04-48374)).

W-AM-K2

STRUCTURE-FUNCTION RELATIONSHIP OF THE DIFFERENT BOVINE α-CRYSTALLIN FRACTIONS. ((T.Aerts,S.Abgar,J.Vanhoudt,J.Clauwaert) Department of Biochemistry, University of Antwerp,Universiteitsplein,1, B2610 Antwerp, Belgium.)

We have examined the different α-crystallin fractions, isolated from bovine eye lens fibre cells and selected on their elution position after gelfiltration.
We have determined their peptide composition by isoelectric focusing and quantifying the amount of protein by Coomassie Blue staining, their molar mass and some hydrodynamic parameters (f/f_0 ratio) by combining equilibrium sedimentation and photon correlation spectroscopy (PCS), their secondary structure by circular dichroism, their thermostability by measuring the circular dichroism as a function of temperature or studying the hydrodynamic parameters by PCS after heating the solutions for 5 min at higher temperatures, their chaperone activity by probing their capability of protecting the β-crystallins against heat-induced aggregation.
The α-crystallin population contains a quite broad distribution of aggregates ranging from 400,000 to 1,500,000 g/mol. The α-crystallins mainly contains 4 peptides αA_1, αA_2, αB_1, αB_2 and some degraded peptides which arise on maturing or aging by specific cleavages of the A and B peptides. Their is a clear relation between the A to B peptide ratio and the molar mass: the larger α-crystallins have a larger A peptide content relative to the B peptide content, as compared to the smaller α-crystallin samples. This explains the increase in the mass of the α-crystallins in older fibre cells and the concomitant predominant A peptide synthesis in these cells.
But their is also a concomitant difference in secondary structure, thermostability of the secondary and quaternary structure and chaperone activity.
So we can conclude that there is a straightforward relation between the peptide composition (αA to αB ratio), the secondary structure and quaternary structure and the chaperone activity of the α-crystallin.

W-AM-K3

SELF-CONSISTENT CALCULATION OF pH DEPENDENT ELECTROSTATIC EFFECTS IN PROTEINS ((Ernest L. Mehler)), Department of Physiology and Biophysics, Mount Sinai School of Medicine, CUNY, New York, NY 10029 (Spon. by V. Brezina)

Recently a new approach was proposed for calculating pH dependent electrostatic effects that uses screened Coulomb potentials for calculating interaction energies, and the integral form of the Born equation with radially dependent dielectric permittivities for estimating the self-energies of the charged groups[E.L. Mehler, *J. Phys. Chem.*, (1996) 100, 16006-16018]. A self-consistent, constrained variational approach was implemented to determine the optimal assignment and distribution of the equilibrium charge state of each titratable residue. A drawback of the method was that only the interaction term could be included in the variational procedure. Here a modified algorithm is presented that includes both the interaction and self-energy terms in the iterative procedure, thus allowing for a more realistic assignment of the equilibrium protonation state. Results from the application of the approach to study the acidotic effect in cardiac troponinC (TnC) suggest that at low pH (i.e., pH of ~6.4 resulting from disease conditions in cardiac tissue) changes in the equilibrium charge state of a few acidic residues weakens Ca^{2+} binding in cardiac TnC. These changes are not seen in skeletal TnC which exhibits much less pH sensitivity. In a second application papain is serving as a structural model for the cysteine protease superfamily to study the effects of inherited mutations in the human cysteine protease, cathepsin K, which cause a lysosomal bone disease, pycnodysostosis [B.D. Gelb, et al., *Science*, in press]. Certain of these mutations in the active site region replace neutral with charged residues and appear to have their adverse effect by shifting the pK's of the Cys-His couple closer to their normal solution values, thereby preventing the initial proton transfer (formation of Cys^- - His^+) that is necessary for catalysis.

W-AM-K4

ENZYME-INHIBITOR ASSOCIATION THERMODYNAMICS: EXPLICIT AND CONTINUUM SOLVENT STUDIES. ((**H. Resat**, T. J. Marrone, and J. A. McCammon)) Koc University, Istinye, Istanbul Turkey 80860 and University of California at San Diego, La Jolla, California 92093-0365.

Studying the thermodynamics of biochemical association reactions at the microscopic level requires efficient sampling of the configurations of the reactants and solvent as a function of the reaction pathways. In most cases, due to the complementary interlocking shapes, loosely connected or disconnected solvent cavities at and around the binding site are formed upon association. Disconnected solvent regions lead to severe statistical sampling problems when simulations are performed with explicit solvent. It has been suggested that such limitations might be overcome by the use of the grand canonical ensemble. In this work, we report the association free energy profile between trypsin and benzamidine calculated using the grand canonical Monte Carlo method to show the advantages of the open ensemble simulations. The free energy profile is also calculated for a continuum solvent model using the Poisson equation, and the results are compared to the explicit water simulations. The comparison shows that the continuum solvent approach is surprisingly successful in reproducing the explicit solvent simulation results. The Monte Carlo results are analyzed in detail with respect to solvation structure and the results are compared to experiments. Accurate prediction of waters bridging the OD groups of Asp189 with amidine groups of the inhibitor and of other experimentally detected internal waters supports the accuracy and advantages of the open ensemble simulations.

W-AM-K5

KINETICS UNDER LOAD: THE PROTEIN A-IMMUNOGLOBULIN G INTERACTION INVESTIGATED USING OPTICAL TWEEZERS. ((**Andrea L. Stout** and Watt W. Webb)) School of Applied and Engineering Physics, Cornell University, Ithaca, NY 14853.

Applying a local stress F to a receptor-ligand bond should, according to Bell (1978), cause an increase in the dissociation rate given by the relationship $k = k_0 \exp(\gamma F/k_B T)$, where k_0 is the stress-free dissociation rate and γ is the effective bond length. To test this theory in the context of a specific interaction, we applied a time-varying load to individual protein A (SpA) - IgG bonds via optical tweezers. IgG molecules were conjugated to microspheres at low densities, and SpA molecules were coupled to glass substrates. Individual binding-detachment events were monitored as an SpA-coated surface was scanned below an optically trapped IgG-bead. This geometry resulted in a 6.7-fold enhancement of the force applied to a bond due to leverage provided by the microsphere. Empirical force calibrations allowed determination of the time-dependent survival probability, S(t), from the measured S(F). This was fit to a theoretical function based on the Bell model. While the data were noisy at low probabilities, they did agree with the model at higher probabilities, yielding, for IgG from several species, values of γ ranging from 1.5 to 3.0 Å and values of k_0 on the order of 10 s^{-1}.

Supported by NIH (RR04224) and NSF (BIR9419978) at the Developmental Resource for Biophysical Imaging and Opto-electronics.

W-AM-K6

KINETIC AND GEL ELECTROPHORETIC EVIDENCE FOR A RAPID REACTION BETWEEN A CHAPERONE TRIMER AND A CHAPERONE – PEPTIDE COMPLEX WHICH PROMOTES PEPTIDE RELEASE. ((C. D. Farr and **S. N. Witt**)) Department of Biochemistry and Molecular Biology, Louisiana State University Medical Center, Shreveport, LA 71130.

The kinetics of the binding of a dansyl-peptide (VSV13*) to the *E. coli* molecular chaperone DnaK was investigated over a range of temperatures (25 to 42 °C) using stopped-flow fluorescence. The experiments were conducted under pseudo-first-order conditions with a fixed concentration of VSV13* (0.1 μM) and varying DnaK (1- 7 μM). At 42 °C, in the absence of added nucleotide, or with added ADP, DnaK-VSV13* complex formation is biphasic, with a growth phase and a subsequent decay phase. The decay phase becomes more prominent as the DnaK concentration is increased from 1 to 7 μM. In contrast, in the presence of added ATP, DnaK-VSV13* complex formation follows simple exponential kinetics, even at the higher DnaK concentrations. Insight into the molecular events which cause the decay phase came from complementary chemical cross-linking experiments. At 42 °C, DnaK (6.0 μM) equilibrates as *three* species (monomers, dimers, and trimers) with or without added ADP, whereas in the presence of added ATP it equilibrates as only *two* species (monomers and dimers). Thus ATP abolishes the subpopulation of trimers and eliminates the decay phase. This suggests that the trimer subpopulation is linked to the decay phase. We propose that following a burst of complex formation after the rapid mixing of the VSV13* peptide with DnaK, a reactive DnaK trimer rapidly binds to a DnaK-VSV13* complex and promotes the release of the bound peptide. Simulations of the this kinetic model yield results that are similar to the experimental biphasic DnaK-VSV13* complex formation traces.

W-AM-K7

ELECTROCHEMICAL CONTROL OF PROTEIN ADSORPTION AND ANTIBODY-ANTIGEN INTERACTION STUDIED BY TOTAL INTERNAL REFLECTION FLUORESCENCE

((**A.N. Asanov**[1,2], L.J. DeLucas[1], P.B. Oldham[2], and W.W. Wilson[2],))
[1]CMC@UAB, Birmingham, AL 35294; [2]MSU, Mississippi State, MS 39762

The objective of this work was to investigate the effect of electrochemical polarization on adsorption behavior of immunoglobulins on the surface of a transparent electrode. The mechanisms of immunoglobulin interactions with solid substrates as well as the ability to control interfacial behavior of antibodies are of great interest for such areas as immunoassays and immunobiosensors, drug release systems, chromatography, etc. Specifically, immobilized antibody activity and kinetics of antibody-antigen interactions depend on surface affinity, strength of adsorption, conformational changes and orientation of adsorbed molecules. In the present study the total internal reflection fluorescence (TIRF) technique in combination with a 3-electrode electrochemical system was used to monitor changes of immunoglobulin adsorption behavior and to probe polarization effect on the kinetics of antibody-antigen interactions. Rates of adsorption and desorption of immunoglobulins at the surface of a transparent SnO_2-electrode, reversibility of protein-surface binding, and structural rearrangements of adsorbed proteins were found to be strongly affected by externally applied polarization. Different electrochemical polarization programs allow modification of adsorption behavior of immunoglobulins and control of antibody-antigen interactions.

W-AM-K8

THEORY OF INTERACTION BETWEEN HELICAL BIOMOLECULES.

((A.A. Kornyshev[†] and **S. Leikin***)) [†]Institut für Energieverfahrenstechnik, Forschungszentrum Jülich, Germany and *LSB/DCRT and ODIR/NIDDK, NIH, Bethesda, MD 20892. (Spon. by D. C. Rau)

A large fraction of biomolecular interactions involves helices. In a number of cases forces have been directly measured (e.g. between DNA double helices, four-stranded guanosine helices, collagen, and some polysaccharides). While longer-range electrostatic double-layer forces are reasonably well understood, this is not so for the last 10-to-20 Å of separation, particularly when the net charge is small but the number of opposite charges on the helices is large (e.g. due to counterion binding). This work builds a theoretical foundation for understanding interactions between various types of helical molecules. In contrast to the traditional approximation of *cylinders* with constant charge density, we present exact analytic solutions for electrostatic and solvation forces between molecules with true *helical symmetry*, with inner cores inaccessible for water and with discrete charged (solvated) groups on them. We focus on the cases when drastic changes in attractive or repulsive interactions are caused by collective, symmetry driven effects. For example, the forces may be qualitatively different for helices with different number of strands, for helices with counter-charges lying on or between the strands, and even for helices with integer or non-integer number of charges per turn. The decay range of the force is often, but not always, determined by the helical pitch. We illustrate several more examples and discuss possible biological implications.

W-AM-K9

CALCULATION OF ASSOCIATION THERMODYNAMICS IN A MODEL PEPTIDE SYSTEM.

((**G.P. Brady** and K.A. Sharp)) University of Pennsylvania, Department of Biochemistry and Biophysics, Philadelphia, PA, 19104-6059. (Spon. by K.A. Sharp)

It has been known for decades that molecular binding is opposed by the famous "association entropy barrier", ΔS^{assn}, produced by the relative immobilization of the binding partners. The range of theoretical estimates of ΔS^{assn} is as large as the binding free energies themselves, while reliable experimental values are almost nonexistent. The present work provides a reliable experimental estimate of ΔS^{assn} for cyclic diglycine (cGG) and assesses of the suitability of current methods for computing binding thermodynamics. Calculations are based upon the decomposition of binding free energy into intra- and inter-molecular energy calculated using Molecular Mechanics, vibrational entropy calculated using Normal Mode Analysis, polar and nonpolar solvation, calculated using Finite-Difference Poisson Boltzmann and surface area free energy models respectively. We apply our procedure to the *gas* ↔ *crystal* ↔ *solution* phase equilibrium of cGG, the thermodynamics of which are known experimentally. Our solvation free energy (-16.4 kcal/mol) and sublimation enthalpy (-24.6 kcal/mol) agree with the experimental values to within 0.2 kcal/mol. The rigidity of cGG enables us to obtain a reliable estimate of -14 eu for the association entropy barrier to transfer of cGG from gas to the crystal. Subtracting exact expressions for S^{trans} and S^{rot} also gives us a reliable estimate of 41 e.u. for the entropy of the crystal lattice. We compute this lattice entropy using three different lattice models and demonstrate that the most rigorous model, Lattice Dynamics, is required to achieve reasonable agreement with the experimental value.

NONLINEAR OPTICAL MICROSCOPY: APPLICATIONS IN BIOLOGY

W-PM-SymI-1 **W. Zipfel, Cornell University**
Multiphoton Excitation of Intrinsic Fluorescence in Cells and in Intact Tissue

W-PM-SymI-2 **S. Fraser, California Institute of Technology**
Imaging Neuronal Targetting, Cell Migration and Synaptogenesis

W-PM-SymI-3 **E. Gratton, University of Illinois**
Mapping Membrane Microdomains and Observing Single Molecule Dynamics

W-PM-SymI-4 **W. Denk, Bell Laboratories, Lucent Technologies**
Functional Imaging of Neurons *in vitro* and *in vivo*